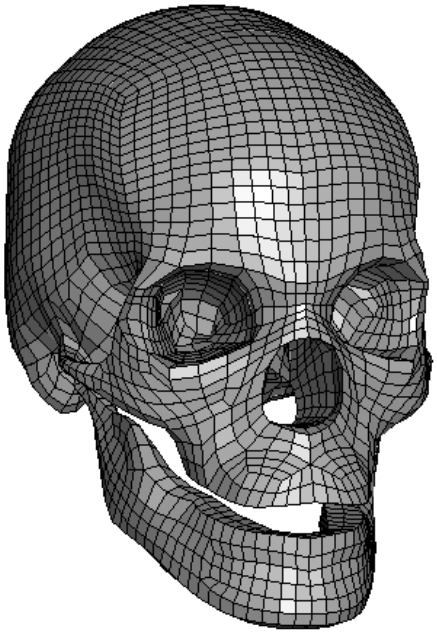

Age-Dependent Material Modelling of the Human Cranium

Predicting Cortical Bone Response Using Bayesian Networks and Experimental Validation

Bachelor thesis in mechanical engineering and biomedical engineering

Anton Back
Stina Granholm
Lukas Larsson
Hanna Viberg

DEPARTMENT OF MECHANICS AND MARITIME SCIENCES

CHALMERS UNIVERSITY OF TECHNOLOGY
Gothenburg, Sweden 2025
www.chalmers.se

Abstract

The risk of skull fracture due to impact increases with age. This project investigates how age affects the mechanical behaviour of cortical bone in the human skull, with the aim of enhancing the accuracy of finite element head models used in fracture prediction. Material properties were derived from experimental data by Wood (1969), which included tensile tests on post-mortem human subjects (PMHS) across a wide range of ages. A Bayesian statistical model was developed in order to analyse the influence of age on strain rate, and material properties such as modulus of elasticity, breaking stress, and breaking strain. The results showed a strong correlation between strain rate and modulus of elasticity, while direct correlations with age were inconclusive due to wide posterior distributions.

Stress-strain curves were generated based on the Bayesian model and used to create age-specific material cards in LS-DYNA simulations. These curves accounted for varying strain rates, allowing more realistic simulation of impacts. To validate the finite element models, simulations were compared to experimental impact data from Raymond et al.(2009), in which PMHS were subjected to blunt impacts to the side region of the head. Fracture risk was evaluated using a survival analysis-based approach for creating risk functions, and compared against experimental outcomes. Although some prediction discrepancies were observed, the trends suggest that aged individuals experience slightly higher strain under the same loading conditions, implying an increased risk of fracture.

The study demonstrates the potential for age-sensitive material models to improve simulations of the human head. It also highlights the need for updated experimental datasets and additional consideration of other anatomical variables such as skull and scalp thickness in future work.

Contents

1 Introduction

This section provides an introduction to the report and aims to establish a understanding of the project.

1.1 Background

Falls can result in various injuries, one of the most serious being head trauma, such as concussions and skull fractures [John Hopkins Medicine, 2025]. Falling is the second leading cause of unintentional injury death, road traffic injuries being first [World Health Organization, 2021], where age is one of the key risk factors.

The world's population is living longer than before [World Health Organization, 2024]. Although this trend began in high-income countries, it is now evident worldwide. According to [World Health Organization, 2024], the number of people aged 60 or older will double by 2050, reaching approximately 2.1 billion. As the human body ages, it can undergo changes such as impaired vision, reduced muscle mass and increased bone fragility [National Institute on aging, 2022]. All these changes contribute to a higher fall risk and higher severity of the outcomes, such as fractures.

The cranium consists of several parts, such as the frontal, parietal, occipital, and temporal bones. The cranial bones consist of an inner and outer layer of compact cortical bone, with a middle layer of porous trabecular bone [Adanty et al., 2021]. The parameters of these materials must be known to perform a proper analysis. With ageing, the cortical bone becomes increasingly brittle and weak [Boskey and Coleman, 2010].

1.2 Problem

Datasets from experiments done to the cranial bone often include key information such as age of each sample and other relevant characteristics. By analysing and correlating these results across multiple samples, it becomes possible to model how material behaviour varies with factors like age. This allows for development of functions that predict stress-strain responses more accurately. Integrating such functions into modern simulation tools could enhance the precision of material behaviour predictions, i.e. more realistic simulation of how the bone responds to impacts or other events. The available models are lacking an understanding of how the bone changes material properties when ageing.

1.3 Theory

Bayesian networks, finite element method and risk functions needs to be understood in order to grasp the content of this report. In the section the basics of each subject is covered.

1.3.1 Bayesian Statistics using Bambi

There are two main doctrines in approaching statistical analysis, frequentative and Bayesian [Goligher et al., 2024]. Frequentative statistical analysis only uses the probability in the observed data, where probability is defined as the likelihood of observing that data in a hypothetical infinite series of repeated experiments. Frequentative analysis does not use any prior assumptions and provides limited information about to which degree the results can be trusted.

In contrast, Bayesian statistical analysis explicitly incorporates prior knowledge or beliefs into the modelling process and updates these beliefs using data through Bayes' theorem, to generate posterior beliefs [Goligher et al., 2024]. The posterior beliefs are represented with a probability distribution over the parameters of interest - the posterior distribution. The posterior distribution encapsulates all available information and allows for a meaningful statement about the certainty of the results, which the shape and spread of the posterior distribution directly communicates.

Example

Consider two generated datasets, containing two variables x and y. In both datasets there is a correlation between y and x, but in *dataset-1* there is a lower spread in the data compared to *dataset-2*, which has a higher spread in the data and contains outliers. The datasets are generated according to Equation 1.1 for *dataset-1* and Equation 1.2 *dataset-2*.

$$y_1 = 2.5x + \varepsilon_1, \quad \varepsilon_1 \sim \mathcal{N}(0, 2^2) \tag{1.1}$$

$$y_2 = 2.5x + \varepsilon_2, \quad \varepsilon_2 \sim \mathcal{N}(0, 6^2) \tag{1.2}$$

The datasets are plotted in Figure 1.1a and 1.1b respectively. In Figure 1.1b the y-axis is in a larger range to include the outliers.

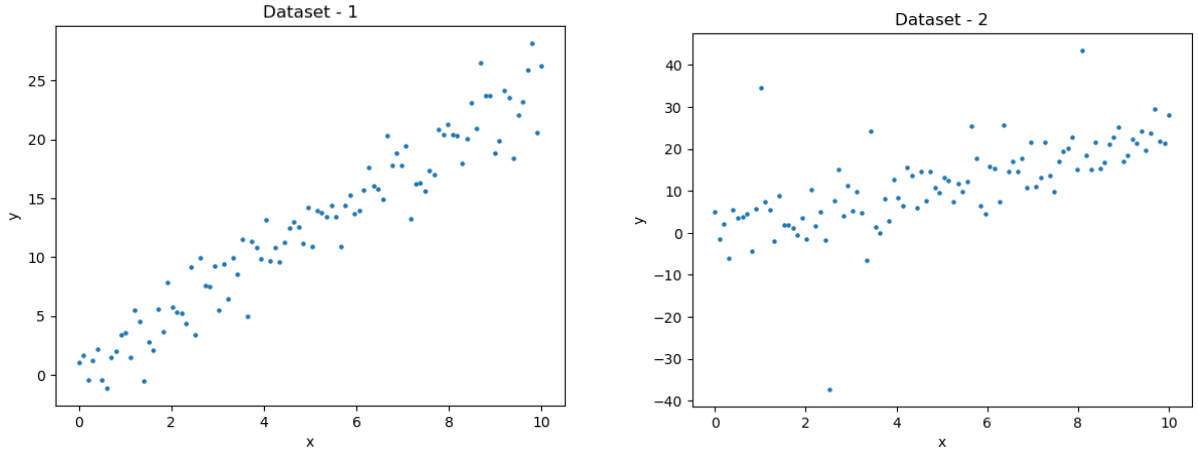

(a) Scatter plot of *dataset-1*

(b) Scatter plot of *dataset-2*

Figure 1.1: Comparison of scatter plots for *dataset-1* and *dataset-2*, note scale on y-axis and the outliers for (b).

Two Bayesian models are fitted on each dataset. Mathematically, these models are described in Equation 1.3. The first line in Equation 1.3 describes that the response variable y is normally distributed with a mean of μ and standard deviation of σ. The second line in the Equation 1.3 describes the linear predictor where α is the intercept (the excepted value of y when $x = 0$, also referred to as the baseline level) and β is the slope (how much y changes per one unit change in x).

$$\begin{aligned} y_{1,2} &\sim \mathcal{N}(\mu_{1,2}, \sigma_{1,2}) \\ \mu_{1,2} &= \alpha_{1,2} + \beta_{1,2} x_{1,2} \end{aligned} \tag{1.3}$$

It is important to consider that all the variables in a Bayesian model are given as probability distributions. Initially, before the model is fitted, the assumed prior distributions are used to describe the variables. The probability distributions describing the variables are updated when the model is fitted on the data and result in posterior distributions for each parameter in the model.

These models are fitted on the examples datasets: *dataset-1* and *dataset-2*. The resulting posterior distribution for the slope: β are presented in Figure 1.2. One model for each dataset is done with a uniform prior distribution, which means that nothing is assumed about the correlation between the two variables. The other model is done with a weakly informative standard prior distribution, which means that an assumption is made of a reasonable value of the slope and its expected spread.

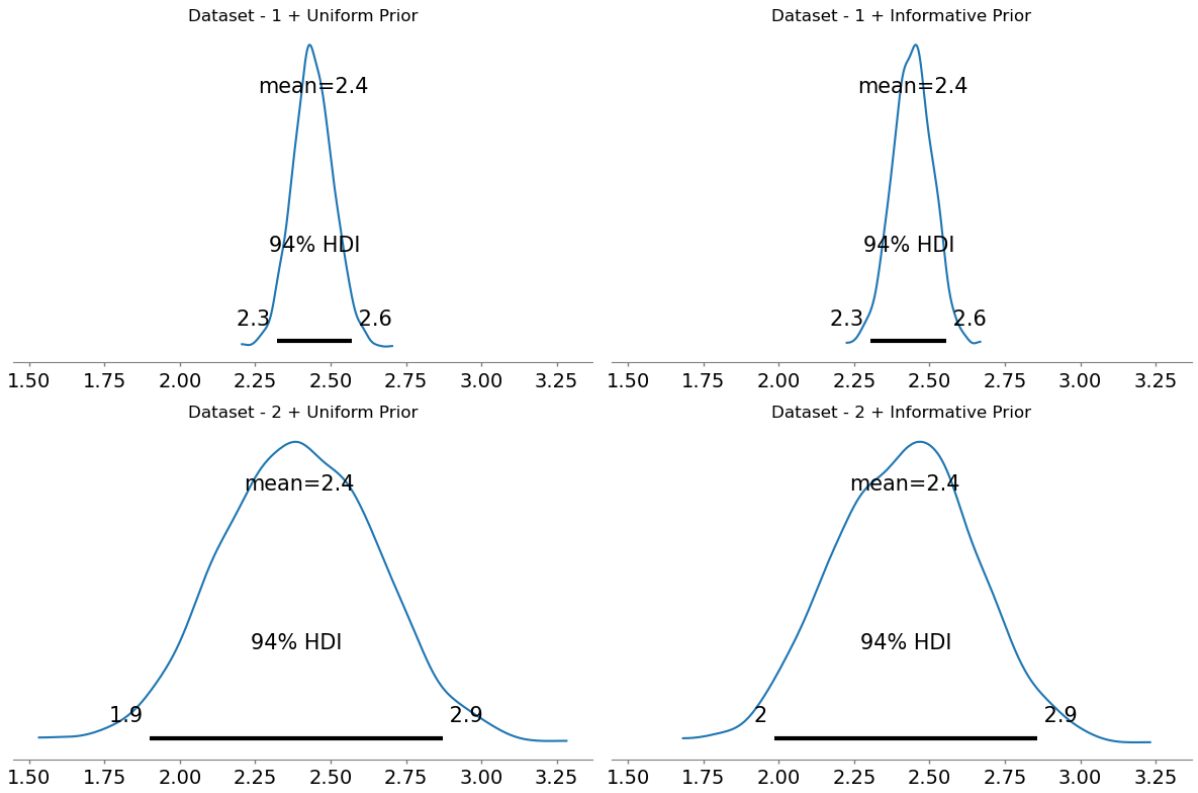

Figure 1.2: Posterior distributions of the slope β for the example models.

In Figure 1.2 a larger spread in the certainty of the results for *dataset-2* compared to *dataset-1* is shown. This can be communicated using the high density interval `HDI`, also presented in Figure 1.2. The `HDI` is the interval which a certain probability the parameter lies within. In this example, for *dataset-1* there is a 94% probability that the slope of the correlation between x and y is between 2.3 and 2.6 for both the informative and uniform prior model, i.e. the `HDI` is 2.3 to 2.6. For *dataset-2* the `HDI` is between 1.9 and 2.9 using a uniform prior distribution, and between 2 and 2.9 using the standard weakly informative prior distribution. Naturally `HDI` is larger for the dataset with more spread and outliers, but both mean slopes are the same at 2.4.

A more complex type of Bayesian models are multilevel Bayesian models, which are useful when analysing datasets containing several levels or categories of data [Edinburgh et al., 2023]. The levels enable the introduction of variation into the data, that would otherwise be unexplainable. For example, consider test score being analysed using Bayesian linear regression. The test scores can be assumed to be correlated with hours studied, but they can also be correlated with school attended. Some schools might provide better education, and consequently achieve higher test scores. Introducing each school as a level within a multilevel Bayesian model allows the model to account for this variability. This allows for each level/school to have its own baseline level. The multilevel model for this example is mathematically described in Equation 1.4.

$$\begin{aligned} \text{Student level: } & y_{ij} = \alpha_j + \beta_1 x_{ij} + \epsilon_{ij} \quad \text{with } \epsilon_{ij} \sim \mathcal{N}(0, \sigma^2) \\ \text{School level: } & \alpha_j = \beta_0 + u_j \quad \text{with } u_j \sim \mathcal{N}(0, \sigma_u^2) \end{aligned} \tag{1.4}$$

In the *Student level*, α_j is the baseline level for a certain school. The variable x_{ij} is hours studied and β_1 is the slope for x_{ij}, i.e the increase in test score for each hour studied. The variable ϵ_{ij} is the deviation of each student's test score from the the model's predicted test score, also called the residual deviation. The residual deviation is assumed to be normally distributed with a standard deviation of σ.

The *School level* defines α_j, that is the baseline level of each school. The variable β_0 is the over all

population intercept, i.e. what the model would predict if all values were 0. The variable u_j is how much each school's baseline deviates from the over all population intercept β_0. u_j is assumed to be normally distributed with a standard deviation of σ_u.

If α_j as defined in the *School level* is substituted into the *Student level*, Equation 1.5 is derived, which describes the multi level model using only one Equation.

$$\begin{aligned} y_{ij} &= \beta_0 + \beta_1 x_{ij} + u_j + \epsilon_{ij} \\ u_j &\sim \mathcal{N}(0, \sigma_u^2) \\ \epsilon_{ij} &\sim \mathcal{N}(0, \sigma^2) \end{aligned} \tag{1.5}$$

Using a multilevel Bayesian model consequently ensures that the estimated effect of study hours is not confounded by variations across schools. Instead the model learns to distinguish variation caused by the different schools and hours studied. Overall, multilevel models improves generalization by regularizing the multilevel effects.

To investigate if a Bayesian linear regression is over fitted a leave one out cross validation (LOO-CV) can be preformed [ArviZ Developers, 2025]. The principal of a cross validation is as following: a data point is removed from the data, and the model is refitted and the model's performance reanalysed. This is done for each data point in the data used to fit the model. Consequently the significance of each data point's effect on the model is assessed. A complete leave one out cross validation is computationally expensive since the model has to be refitted for each data point in the model. A Pareto-smoothed importance sampling leave one out cross validation score (PSIS-LOO-CV) estimates the LOO-CV without the need for repeated model fitting and is therefore less computationally expensive.

Bayesian interference relies on stochastic algorithms, thus the algorithms produce satisfactory result only when they have run long enough i.e when they have converged [ArviZ Developers, 2025]. A potential scale reduction factor ($\hat{R}$) can be used as a diagnostic tool to verify that the algorithms used to fit the Bayesian model converged. $\hat{R}$ approaching 1 implies that the algorithms have converged.

1.3.2 Risk Function

There are many various ways a risk function can be utilized [Statistics How To, nd]. A function often takes observations as input and produces, for example, a decision or an estimate as output. The risk function can be used when data has unknown estimators and can assist in evaluating different estimators while considering both variance and biases.

To develop a risk function for injury risk caused by a car crash test, a number of steps should be followed according to the ISO standard [International Organization for Standardization [ISO], 2014]. Some steps can be added or put together. Example of a project using a modified step by step to create risk functions can be read in the report by [Larsson et al., 2021]. In the following list an example of steps can be seen.

1. Acquire data.
2. Assign censor status
3. Identify the reason for the condition
4. Divide the data by reasons for the condition
5. Using a model to identify significant parameters.
6. Check influential observations.
7. Distribution selection for the data.
8. Build a Injury Risk Curves (IRC) with selected distribution.
9. Plot IRC curve.

10. Check quality at quantiles.

The first step (step 1) is to acquire data to build the risk function on. This data should consist of information about the condition under investigation or the subject evaluated by the risk function. Step 2, in this step the data gets assigned censor status, binary zeros and ones, for the condition under investigation. For example, zero and one represent not sick and sick, or zero and one represent alive and deceased. Step 3, the reasons for the condition is investigated and if there is different reasons the data is split in groups with the various reasons as dividers in the next step (step 4), e.g., different groups for deceased from sickness or accident.

In step 5, a model for identifying influential observations are used, for example COX regression [GraphPad, nd]. The first thing that Cox regression preforms is a hazard function that calculate the failure (or break, dead, etc.) for certain data over time (can be spans other than time such as tension). The COX regression then uses a function that calculates which variables have an influence over the data and hazard calculation, while enabling adjustments to the variables. Step 6, uses a model like Difference in BETAs regression coefficients (DFBETAS) to identify where in the dataset the significant parameters come from by calculating thresholds [Goldstein-Greenwood, 2022]. The theory behind DFBETAS is about seeing the changes in regression coefficients β when removing observations from a data set and how it effects the significant parameters. Different thresholds can be used when calculating the more influence data points, the most common used is $\frac{2}{\sqrt{n}}$ as it varies depending on how many data points there are. If some data points are over the threshold, those specific data points contribute more than the remaining data. A decision can then be made whether to keep the data as is or remove data points that are considered outliers.

In the next step (step 7), models are fitted to the data to find a suitable distribution, some of the most commonly used models for distribution are: Weibull, log-normal and log-log. The different models are compared with each other to see which one fits the data best [Davidson-Pilon, nd].

In step 8 the Injury Risk Curves (IRC) are built by fitting the selected distribution with the significant parameters and data. The IRC is plotted in step 9, to enable interpretation of the results and comparison of the significant parameters at different values. The last step (step 10) is to evaluate the quality of the curve, the width of the Confidence Intervals (CI) at different risk percentages is used for the quality evaluation, i.e. difference between the upper and lower value.

1.3.3 Finite Element Method - FEM

The finite element method (FEM) is a powerful numerical technique for solving problems in engineering and mathematical physics [Zienkiewicz et al., 2013]. It is widely used to simulate physical phenomena such as structural deformation, heat transfer, and fluid dynamics. FEM can be divided into different concepts: discretization, shape functions, element matrices, global system, boundary conditions, and solvers.

Discretization of Domain
Discretization of the domain is the process of dividing the problem domain (geometry) into smaller and simpler pieces called finite elements [Zienkiewicz et al., 2013]. The domain can be 1D (line), 2D (surface), or 3D (volume). The finite elements are connected at discrete points called nodes. The process of generating elements and nodes is called mesh generation. Common element shapes are triangles, quadrilaterals, tetrahedra, and hexahedra.

Selection of Shape Functions
The next step in the FEM methodology is to implement shape functions. Each element uses shape functions to interpolate the unknown field variable (e.g., displacement) over the element. Shape functions are usually polynomials, and their form depends on the element type.

Derivation of Element Matrices
For each element a local stiffness matrix (K^e) and load vector (f^e) is derived based on the governing differential equations (e.g., from elasticity) . This is done by integrating over the element domain.

Assemble into Global System
All of the local stiffness matrices are then assembled into a global stiffness matrix (K) and the load vectors into a global load vector (f) using nodal connectivity. Together with a unknown vector (a) the assembled system can look like Equation 1.6.

$$Ka = f \tag{1.6}$$

Apply Boundary Conditions
To make this problem solvable, some boundary conditions must be applied. For example, by specifying either the value of the unknown (e.g., fixed displacement) or the derivative or flux (e.g., applied force). The boundary conditions are incorporated into the global system by modifying the matrix and vector appropriately.

Solvers
With the global matrix, the load vector and the boundary conditions, the system (Equation 1.6) is solved using linear algebra. There are two main solvers that can be used: implicit or explicit. The biggest difference between the two is the time integration; the implicit method solves a matrix system at each time step whereas the explicit method does not. The explicit computes the next state directly from current/previous values and the implicit by solving the equations involving future unknowns. These differences makes the explicit method more suitable for rapid dynamics and problems with short duration and the implicit more suitable for slow-moving problems and longer time-steps in the calculation.

In FE modelling, fracture cannot be predicted directly; instead, a failure theory must be applied to assess the likelihood of failure [Keyak and Rossi, 2000]. Common examples of such theories include distortion energy, maximum normal stress, and maximum normal strain. Using these theories, the risk of fracture can be evaluated based on calculated values and compared or correlated with results from physical experiments.

There are finite element models of the human body available, called human body models (HBM). The models can be used to simulate different scenarios, such as collision, fall, and penetration. Data from the simulation can be extracted and conclusions can be drawn. Many models represent a 50th percentile human, for example a model by DYNAmore [DYNAmore, nd] and models by VIVA+ [Viva+, 2024]. Other sources have started to develop different models based on different ages [Global Human Body Models Consortium, nd, Toyota, nd]

A software called LS-DYNA was used in this project to solve FEM problems. LS-DYNA is a multiphysics solver widely used in the industry for applications such as occupant safety, impact and penetration, drop-tests [Ansys, 2025]. It operates using keyword files that define the simulation setup. For example, material properties, mesh configuration (nodes and elements), boundary conditions, and output parameters (e.g., reaction forces and energy). The keyword files can be created and edited in a preprocessor like LS-PrePost or some text editor tools like Visual Studio Code, often with the aid of Python scripts to automate simulations. The primary output is a binary file that can be analysed in LS-PrePost or by third-party tools like Dynasaur. Other outputs, such as animations can also be generated.

1.4 Purpose

The purpose of this study is to find how the mechanical properties of bones change dependent on age, and implement those changes into a FEM simulation. The effect age has on the mechanical properties of the skull bone needs to be further understood and models are needed that describe this effect. The results of such models will be implemented in modern FEM software and enable the possibility to account for age when performing simulations of head injury. The risk function that estimates the risk of fracture for the results of such simulations also needs to account for age. Finally, using the risk function on the result of FEM simulations accounting for age, head injuries in elderly people can be further understood and eventually prevented.

There are lots of different projects and companies that are using HBM with FEM software that would greatly benefit from implementing age. In addition to this, the results from this project could also be used in further studies where simulation tools for development of countermeasures will be developed.

1.5 Limitations

This project was conducted during the spring of 2025, and was done at 50% speed. Therefore, time was one of the biggest limitations. Many of the theories and concepts were new and the software was previously unknown for the project group. In order to be able to get a result, material parameters for every ages were not conducted. Instead material for a 50 year-old individual and an 80 year-old individual was created for both female and male. Some factors with a possibility of affecting the probability of fracture had to be skipped due to the time limit, (e.g., scalp and skull thickness).

All data used in this project was taken from previous experiments. This meant the project had to be based on existing data and could not be formed to be project specific. Some of the data used is from over 50 years ago, since then, the methods and measuring equipment has developed.

The limitation in time and knowledge in LS-DYNA made the final simulations run with a material parameter called MAT024. MAT024 is mostly used for metals and does not perfectly correlate to the properties of a human bone and therefore, might have an affect on the results.

Due to lack of data and time, all data measured for the trabecular bone was removed from the dataset for fitting the Bayesian models. The trabecular bone has other material properties than the cortical bone and can therefore not be combined.

2 Method

This project consists of four parts, Bayesian modelling to predict material properties, implementing the prediction into the FEM software, validating the material by replicate a physical experiment, and building a risk function dependent on age. Bayesian statistics was used to model how the material properties of skull bone changes with different parameters (age, sex, etc.). The Bayesian models predicts modulus of elasticity, breaking strain and breaking stress, from which complete stress-strain curves are generated using a mathematical function. By replicating a tensile test in LS-DYNA, the output from the Bayesian network was verified. In order to validate the material, another replication of a study was simulated. The post-mortem human subjects (PMHS) in the study were impacted by an impactor and whether fracture occurred or not was noted. From the simulations, the strain at the experiment fracture point was extracted. This value was used to see the probability of fracture with a risk function. The risk function was calculated and developed using data from a study. The flow of data, functions, and models can be visualized in Figure 2.1. In the following subsections, a deeper explanation of the methodology is given.

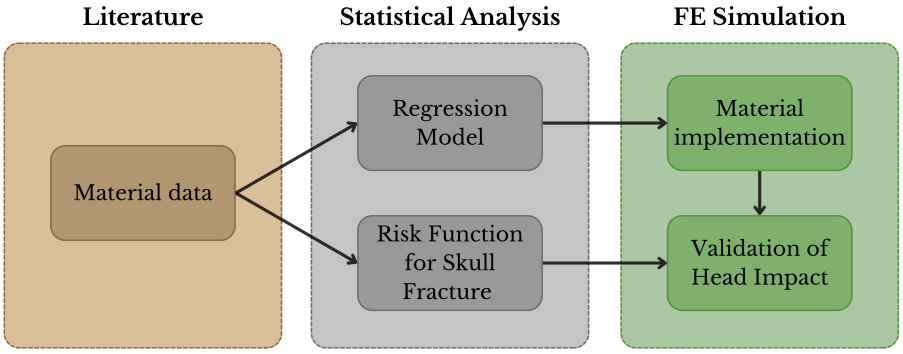

Figure 2.1: Flow chart shows the flow of data and other outputs in the project.

2.1 Cortical Bone material properties

To understand how the material properties of skull bone changes with age and other important parameters Bayesian regression models were used. This section provides an introduction to the data used and a mathematical description of the models. Furthermore the complete stress-strain response were estimated using the material properties.

2.1.1 Exploratory Data Analysis

The data used in this project to model the properties of skull bone material is entirely provided from one study done by Jack Wood [Wood, 1971]. In the Wood study several tensile tests were performed on different part of the skull bone with a range of strain rates, see Equation 2.1 for definition of strain rate. The tensile tests were performed on small uniform samples carved out of the skull bone of cadavers. The samples were pulled under tension until the material broke. The shape of the these samples was similar to the shape of a dog bone, they are hence sometimes referred to as dog bone samples.

$$\text{Strain rate} = \dot{\epsilon} = \frac{\text{dStrain}}{\text{dTime}} = \frac{\mathrm{d}\epsilon}{\mathrm{dt}} \tag{2.1}$$

During the duration of the test the elongation of the sample was measured together with the force required to induce the tension. The force applied to the sample was divided by the smallest cross section area of the sample to calculate the engineering stress. The elongation of the sample was divided by the original length of the sample to calculate the engineering strain. The relationship between engineering strain and engineering stress during a tensile tests describes the material properties of skull bone material for a certain strain rate. The engineering strain and engineering stress measured during a tensile test are often plotted against each other to visualize the material properties for a certain strain rate. One

example of a stress-strain curve from Woods study is in Figure 2.2. The two stress-strain curves shown are each averages of three tensile tests preformed at the same nominal strain rate, exactly which three tests the curves are an average of is not stated explicitly in the report.

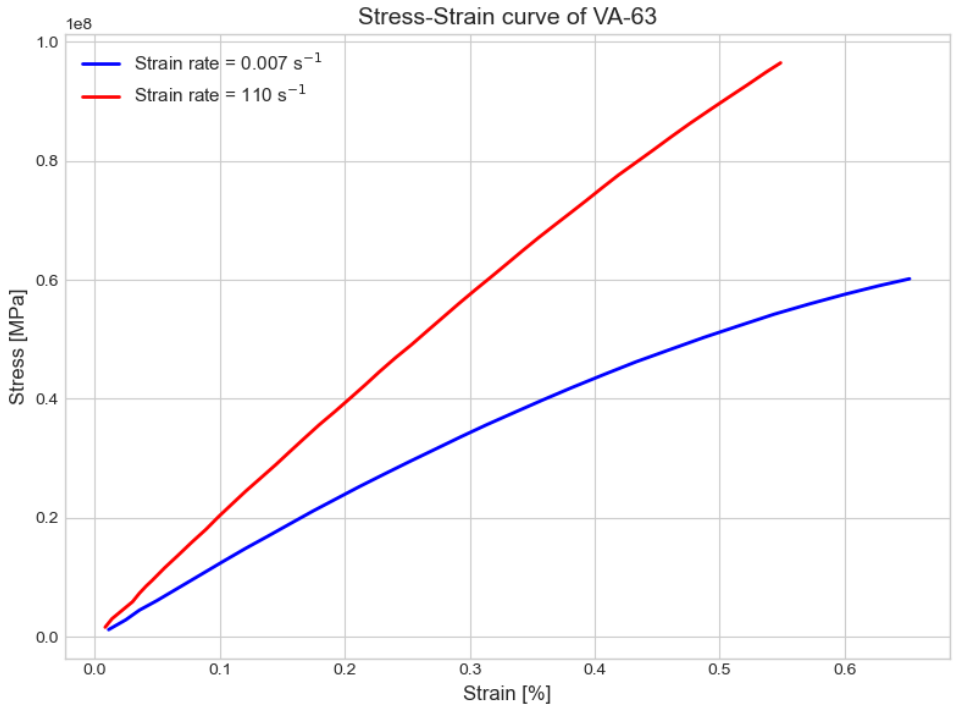

Figure 2.2: Averaged Stress-Strain curves from three tensile tests preformed at the same nominal strain rates [Wood, 1971].

The material properties of the skull under tension are strain rate dependent and more complex than typical engineering materials [Wood, 1971]. Strain rate dependency means that the properties of the material under tension changes with the speed of which the tension is applied. Therefore, it is important to consider that a stress-strain curve only represent the materials properties during tension for one specific strain rate. To fully describe the material properties several stress-strain curves are needed for different strain rates.

The tensile tests were preformed on a total of 142 bone samples taken from 29 cadavers of different ages ranging from 25 years to 95 years and of both sexes (134 male and 8 females) [Wood, 1971]. Samples were taken from different parts of the skull: the parietal (94 samples), temporal (9 samples) and frontal (39 samples). Also both outer layer cortical bone (114 samples), inner layer cortical bone (18 samples) and trabecular bone (8 samples) were tested. The strain rates used in the tensile tests ranges from $0.003sec^{-1}$ to $130sec^{-1}$.

Complete stress-strain curves are published only for two samples [Wood, 1971]. The rest of the data presented from the tensile tests are not the complete stress-strain curves but values of specific properties describing the stress-strain curves. These properties are breaking stress, breaking strain, modulus of elasticity and energy to failure. Breaking stress and breaking strain are defined as stress and strain at which the sample broke. Modulus of elasticity is defined as the slope of the secant at the strain value 0.2%.

Modulus of elasticity, breaking strain and breaking stress are needed to construct a material curve and will be referred to as the material defining properties. To predict the material defining properties, initially the data had to be cleaned and analysed to understand what could be correlated with the material defining properties.

The data concerning the material defining properties is published in [Wood, 1971] in the form of several

tables. The data was copied manually from the tables I, Appendix B and table VI into one table using excel. The data was converted from imperial units to SI units, specifically breaking stress was converted to MPa, modulus of elasticity was converted to GPa. This data is referred to as the original dataframe. Furthermore, all the 8 tests preformed on the softer trabecular bone were removed from the dataset. The log_{10} of the strain rate was also calculated and stored in a separate column in the dataframe, since the strain rate ranged between $0.003sec^{-1}$ and $130sec^{-1}$ and the range needed to be compressed.

To analyse which parameters might be correlated with each other several scatter plots of the data were generated. The material defining properties were plotted in a scatter plot against age with a gradient of strain rate and dot shape indicating if the test was preformed on outer or inner layer cortical bone. The material defining properties were also plotted in scatter plots against strain rate. Additionally, breaking stress and breaking strain were plotted against modulus of elasticity.

2.1.2 Fitting the Bayesian models

In this study, the high level Python library Bambi is used to create, evaluate and compare different Bayesian models [Bambi Developers, 2025]. Bambi is built on top of the probabilistic programming library PyMC. For visualisation the library ArviZ is used [ArviZ Developers, 2025].

The Bayesian model for modulus of elasticity was initially fitted. The mathematical equations describing the model is presented in Equation 2.2. The data used to fit the model was the original dataframe, but all the rows containing missing values for strain rate, age or modulus of elasticity were removed (dataset 1).

$$\begin{aligned} \text{Youngsmodulus}_i = \beta_0 &+ \beta_1 \cdot \text{log\_strainrate}_i + \beta_2 \cdot \text{Age}_i \\ &+ \beta_3 \cdot \text{Sex[M]}_i \\ &+ \beta_4 \cdot \text{Part2[T]}_i + \beta_5 \cdot \text{Part2[P]}_i \\ &+ \beta_6 \cdot \text{Bone[IT]}_i + \beta_7 \cdot \text{Bone[OT]}_i \\ &+ u_{j[i]} + \epsilon_i \end{aligned} \tag{2.2}$$

$$u_j \sim \mathcal{N}(0, \sigma_u^2), \quad \epsilon_i \sim \mathcal{N}(0, \sigma^2) \tag{2.3}$$

The names used in Equation 2.2 are the same names used in the definition of the model and consequently the same names that will appear in plots. To clarify *Youngsmodulus* is modulus of elasticity and is a continuous variable. The variable *log_strainrate* is the log_{10} of the strain rate and is also continuous. The variable *Bone* is categorical and corresponds to inner or outer cortical bone (IT or OT). The variable *Part2* is categorical and corresponds to parietal, temporal or frontal (P, T or F). The variable *Sex* is categorical and corresponds to female or male (F or M). The categorical variables works as following: if, for example, the bone is from the parietal part of the skull implies that $\text{Part2[T]}_i = 1$ and the $\text{Part2[P]}_i = 0$. The model is multilevel with each cadaver being a level. The variable $u_{i[j]}$ is the variation of the intercept at the level of each specimen (cadaver), which is assumed to be normally distributed around zero with a standard deviation of σ_u. The variable ϵ_i is the residual variation also assumed to be normally distributed with a standard deviation of σ.

The posterior distributions were plotted for the following parameters: the intercept β_0, the slopes of each variable β_1 to β_7, the standard deviations σ_u and σ, and the u values for each specimen. The $\hat{R}$ value was calculated for each of the mentioned parameters. A PSIS-LOO-CV score was also calculated for the model. Furthermore, for each variable the probability of its corresponding β being either positive or negative was calculated.

The models for breaking strain and stress were almost mathematically identical to the model predicting modulus of elasticity, except modulus of elasticity was added as a continuous input variable. The data used was dataset 1, but all the rows containing missing values for breaking strain and breaking stress were removed (dataset 2). The same evaluation plots and scores were generated for the models of breaking strain and stress as the the model of modulus of elasticity.

A function was created that predicts the material defining properties using the Bayesian models. The

function takes the following input parameters: strain rate, age, sex, inner or outer cortical bone, and part of the skull. The function firstly predicts the modulus of elasticity using the input parameters, thereafter it predicts the breaking stress and strain using the predicted modulus of elasticity together with the input parameters. It preforms all predictions using the mean of the corresponding slopes and intercepts.

2.1.3 Generating complete stress-strain curves

The generating of complete stress-strain curves using the material properties was done by fitting curves according to the following assumptions:

1. The curve begins at the origin.
2. That the curve is completely linear for strains below 0.2%.
3. The curves follows a polynomial of either the second or third degree after 0.2% strain until the end of the curve.
4. The slope at the beginning of the polynomial is exactly the modulus of elasticity.
5. For the case of the third degree polynomial, the second derivative of the polynomial at 0.2% is exactly zero.

This is described mathematically for the second degree polynomial $\sigma_2(\epsilon)$ in Equation 2.4 and for the third degree polynomial $\sigma_3(\epsilon)$ in Equation 2.5. σ = Stress, ϵ = Strain, σ_B = Breaking stress, ϵ_B = Breaking strain, E = Modulus of elasticity.

$$\sigma_2(\epsilon) = \begin{cases} E\epsilon & \text{if } \epsilon < 0.2 \\ a\epsilon^2 + b\epsilon + c & \text{if } \epsilon \geq 0.2 \end{cases} \tag{2.4}$$

$$\sigma_3(\epsilon) = \begin{cases} E\epsilon & \text{if } \epsilon < 0.2 \\ a\epsilon^3 + b\epsilon^2 + c\epsilon + d & \text{if } \epsilon \geq 0.2 \end{cases} \tag{2.5}$$

Equations 2.4 and 2.5 where solved for the polynomial constants a, b, c and d using the conditions described in Equation 2.6.

$$\begin{aligned} \sigma_{2,3}(0.2\%) &= E \cdot 0.2\% \\ \sigma_{2,3}(\epsilon_B) &= \sigma_B \\ \sigma'_{2,3}(0.2\%) &= E \\ \sigma''_3(0.2\%) &= 0 \end{aligned} \tag{2.6}$$

The solution from Equation 2.4 and 2.5 was used to generate four validation curves, using the same material defining properties as for the published stress-strain curves for VA-63 in Figure 2.2. Two curves where generated for each of the two published curves, using the same material defining properties corresponding to the published curves. One curve using the second degree polynomial and one using the third degree polynomial where generated for each published curve. These curves where then plotted in the same plots as the curves published by Jack Wood and compared. A Root Mean Square Error (RMSE) score was calculated between the curves generated by Equation 2.4 and 2.5 and the curves published by [Wood, 1971]. The degree of the polynomial resulting in the lowest RMSE score was used in a function that creates a complete stress-strain curve, using the material defining properties.

A total of 20 curves were generated for calibrating the material card. Firstly, the material defining properties were predicted using the function for predicting the material defining properties. Material properties were predicted for combinations of five strain rates ($0.01sec^{-1}$, $0.1sec^{-}1$, $1sec^{-1}$, $10sec^{-1}$,

$100sec^{-1}$), two ages (50 years and 80 years), and for sex (female and male). All the combinations were predicted assuming outer cortical bone and the effect of the bone location in the skull was averaged out. Thereafter, the function for generating complete stress-strain curves were used to generate 20 complete stress-strain curves for the FEM implementation.

2.2 Risk function for Cortical Bone fracture

In this project the risk function will be used as prediction tool based on data about the skull and its bone mechanics to calculate the risk of fracture for different strain values. To generate a risk function the following steps were used:

1. Data processing.
2. COX regression to see significant parameters.
3. DFBETAS to check influential observations.
4. Distribution selection for the survival data.
5. Builing IRC curve with selected distribution.
6. Plotting IRC curve.
7. Checking quality at quantiles.

To begin with the risk function the first (step 1) is to process the data from [Wood, 1971]. Dataset 2 described in Section 2.1.2 was used to create the risk functions. To increase the comprehension of the data and how the content in the dataset relate to each other, the data was visualized by plots in different configurations. To get data with less outliers the mean was calculated.

To calculate the mean for each specimen, the data of each specimen was divided in to different groups. To avoid mixing data, the data was divided by place from the skull, as in frontal, parietal and temporal, and if it was outer or inner cortical bone. The true elastic and true plastic strain were important for the comparison in the end of the project to work properly between the result from the risk function and the simulations. Since the data in Wood is from a tensile test, the stress and strain were given in engineering values. Continued processing of data was done to get the true strain and stress from the mean values of the test data from Wood, Equations 2.9 and 2.10. With the true stain and stress, the true plastic strain was calculated with the Equation 2.11. The true elastic strain was calculated in Equation 2.7,

$$\text{elastic strain} = \frac{\sigma}{\mathrm{E}}, \quad 0 < \sigma < \text{yield stress} \tag{2.7}$$

For a complete understanding and comparison the elastic and plastic strain were also calculated using the engineering strain and engineering stress values from Wood.

The true elastic and effective plastic (true) strain was calculated using true strain and true stress. Engineering elastic and engineering plastic strain calculated using the engineering strain and engineering stress values from Wood.

In step 2, COX was used to highlight parameters that were significant to the risk function. For a parameter to be classed as significant it's Pr value had to be under 0.05. For step 3, the significant parameters from step 2 were evaluated using DFBETAS. With DFBETAS a "confidence" interval was introduced to see if there were any outliers. If an outlier was identified, it had to be evaluated whether to be removed or not. An important step for the production of the risk function is to understand what data point influence the significant parameters. To calculate an appropriate threshold Equation 2.8 was used, where n is the number of data points.

$$\text{Threshold} = \frac{2}{\sqrt{n}} \tag{2.8}$$

The hazard analysis and fitting of the distribution model for the data is done in step 4, various distribution models were fitted to the data with the significant parameters in the calculation. A model with a lower Akaike information criterion (AIC) value is considered better. The tested distribution models was as followed: Weibull, log-normal and log-log. To verify the AIC value, the data and the different models were plotted. In the next step (step 5) the a IRC curve was fitted with the selected distribution from step 4, the significant parameters from step 2 and dataset 2. The distributions equations coefficients adjusted to fit the data and the significant parameters.

In step 6, the IRC curve was plotted so the curve can be interpreted and used to compare with other data, such as simulation data. The steps 2 to 6 were done for true plastic strain, true elastic strain, plastic strain, elastic strain, and total breaking strain. Lastly, (step 7) the IRC curves quality at quantiles was evaluated. The evaluation is done by calculating the width of the CI. The width corresponding to the difference between the upper and lower CI value. The width is then compared to a chart that determines what a good curve is. (The specific chart can be seen in Appendix E, Table E.1).

2.3 LS-DYNA implementation of Cortical Bone

The material properties that were predicted had to be translated into information that LS-DYNA could implement in the simulations. This was done by creating material cards and implementing the generated curves. Each material card included different types of keywords to define material behaviour. The material keyword defines the material definition with its essential properties, modulus of elasticity, mass density, and Poisson's ratio. The material definition also references curve keywords which are called *DEFINE_CURVE. The curve is an X and Y curve where the X axis is the effective plastic strain and the Y axis is the true stress. This defines what stresses occurs at what strains. Finally, a define table keyword was referenced to map each curve to its corresponding strain rate, allowing interpolation between curves based on the strain rate experienced during the simulation. Both the curves and the table were used in the chosen material definition to create the material card. The material cards were created automatically using a python script that were written specifically for this project with the correct format.

The different LS-DYNA material keywords have different ways of calculating the behaviour of the material before the yield point and how the provided curves are implemented. The material keyword used was *MAT_PIECEWISE_LINEAR_PLASTICITY_(TITLE) (024), (MAT024). MAT024 is linear until the yield point, imitating the behaviour of metals. The linear part is based on the modulus of elasticity. MAT024 was chosen since it is widely used for different applications in modern time. For example, in the VIVA+ model and for crash simulations.

The implementation of the material was done by firstly simulating a dogbone sample with curves generated from the Wood data [Wood, 1971]. The curves aimed to give the same results as sample VA63 did in the report. This would enhance the credibility of both the stress-strain curves and the simulation outputs since there would be confidence in running the simulation and getting correct outputs. When sample VA63 was verified, material properties predicted by the Bayesian regression were used to generate curves for ages of 50 and 80, both for male and female. Specifically, five stress-strain curves were defined for each material card, each corresponding to a different strain rate. The strain rates used to generate curves were 0.01, 0.1, 1, 10, and 100 s^{-1}, as outlined in Section 2.1.3.

To ensure that the correct strain rate occurred during the simulation, the strain rate was estimated by calculating the difference in velocity divided by the difference in x-coordinates. The operating functions within the LS-PrePost graph plotter were used for the calculations. This was done across nodes the nodes 778 and 765 located in the region with the smallest cross-section. The variables in LS-DYNA that were adjusted to ensure that the correct strain rates occurred were the displacement [mm] at the end of the simulation and the time [ms] for the displacement. This translates to how fast the dogbone sample was elongated. Since there are 2 unknown variables, time and displacement, and one equation in the strain rate Equation 2.1, trial and error was used to find the correct strain rate.

To get a greater understanding on how MAT024 could potentially work, a simulation were also done for strain rate 100 with the correct modulus of elasticity and then with the modulus of elasticity for strain rate 1. This test was done to see how MAT024 worked with its linear plasticity definition.

The generated curves had to be verified to ensure the correct material implementation and simulation results. This is done by calibrations and modifications made on both the material card and the generated curves. Before using the generated curves in LS-DYNA, the curves had to be recalculated from engineering stress and engineering strain into true stress and true strain values. This is because the data from [Wood, 1971] was presented as engineering stress and strain, whereas the FEM software LS-DYNA requires true stress and strain values [DYNAmore GmbH, 2002]. The difference between the two is that engineering values does not take the deformation during the test into consideration. The stress-strain curve of a tensile test with engineering values will result in a curve where stress decreases at the end of the curve, while a result with true values will have the stress increasing at the end of the curve. To convert the values to true values, Equations 2.9 - 2.11 were applied to the result.

$$\text{strain}_{(\text{True})} = \text{LN}(\text{strain}_{(\text{engineering})} + 1) \tag{2.9}$$

$$\text{stress}_{(\text{true})} = (\text{stress}_{(\text{engineering})}) * \exp(\text{strain}_{(\text{true})}) = (\text{stress}_{(\text{engineering})}) * (1 + \text{strain}_{(\text{engineering})}) \tag{2.10}$$

$$\text{effective plastic strain} = \text{total strain}_{(\text{true})} - \frac{\text{stress}_{(\text{true})}}{\text{E}} \tag{2.11}$$

$$\text{strain} = \text{plastic strain} + \text{elastic strain} \tag{2.12}$$

Strain = elastic strain + plastic strain From the true strain, the effective plastic strain can be calculated with with Equation 2.11. While calculating the effective plastic strain, there can be negative values in the results. When values exceeds 0, the strain has a plastic part, i.e. the yield point is located at the value closest to 0. Negative plastic strain indicates that the plastic part is negligible since the curve then is in its elastic part as seen in Equation 2.12. Before the curves were used, the curves were extrapolated to make all curves end at the same x-value. This helps with the simulation results and make it more precise [DYNAmore GmbH, 2020].

The results of the dogbone sample simulations were then controlled for each age and sex so that the results were reasonable. The 4 material card, with the corresponding material definition, curves and table, could thereafter be implemented for the HBM.

2.4 Head Impact Simulation

The purpose of the validation is to determine the strain level at which fracture occurs. This was done by recreating a study, using human body models (HBM) to replicate the physical experiment. Information about the initial HBM used can be found in Section 2.4.1 and a summary of the study can be found in Section 2.4.2. The results of the study was compared with output from the simulations. As mentioned in Section 1.3.3, the FEM simulation itself can not determine if fracture occurs. Instead a failure theory was implemented, maximum strain was used in this project. Further information about the validation of material can be read in Section 2.4.3.

2.4.1 Human Body Models (HBMs)

VIVA+ is a line-up of open source finite element models of vehicle occupants and standing road users [Viva+, 2024]. Their baseline model is an average female, average defined as 50th percentile. In addition to the baseline, Viva+ maintains three other models: average male, standing average female, and standing average male. The VIVA+ models were developed during the VIRTUAL project, led by the Swedish National Road and Transport Research Institute between 2018 and 2022. Since the project's conclusion, a dedicated team of four members has continued to maintain and improve the models.

Model validation is a crucial part of the development process to ensure the models accurately represent human biomechanics. VIVA+ includes a comprehensive validation catalog in which experimental data is used to verify different body regions of the models [Viva+, 2024]. For the head, a study by Raymond (2009) was utilized. In this validation, only the head components of the FE models were evaluated [Viva+, 2025]. The mass of the head differs between the female and the male models. Specifically, the head mass is 3.82 kg for the female model and 4.42 kg for the male model [Viva+, 2022].

2.4.2 Summary of Head Impact Experiment

Raymond's study aimed to understand how likely it is for the skull to break when hit by a blunt object in the side of the head (the temporo-parietal area) [Raymond et al., 2009b]. The study involved seven post-mortem human subjects (PMHS), four females and three males, aged between 55 and 75 years. The head masses for the subjects ranged from 3.1 to 3.48 kg for females and from 2.98 to 4.3 kg for males. Detailed information about each subject, including gender, age, head mass etc., is summarized in Table 2.1.

Table 2.1: Summary of information about all PHMS from Raymond study and the velocities of impact. L/R meaning impact on left or right side of the skull.

PMHS ID	**Gender**	**Age**	**Head Mass [kg]**	**Velocity (L/R)[m/s]**	**Skull Thickness (L/R) [mm]**	**Scalp Thickness (L/R) [mm]**
2426	M	69	3.26	32.1/22.1	3.6/3.6	7.0/7.0
2427	M	57	2.98	34.2/23.4	6.1/6.3	5.0/5.0
2904	M	74	4.30	31.9/17.3	5.2/5.6	8.0/8.0
2908	F	73	3.48	35.1/19.6	4.2/4.1	7.0/9.0
2939	F	63	3.28	16.3/34.4	6.0/6.0	15.0/16.0
2965	F	75	3.42	18/35.2	3.9/5.0	7.0/7.0
2978	F	55	3.10	19.5/32.4	4.5/3.5	6.0/6.0

Each subject was impacted twice - once on the left side and once on the right- at velocities of approximately 20 m/s and 35 m/s (low and high speed), yielding data from 14 total impacts. The impacts were delivered slightly behind the temple, more specifically, 25 mm anterior to the external acoustic meatus and 35 mm superior to the Frankfurt plane. The impactor used had a diameter of 38mm and a mass of 103 g. Fracture occurrence was assumed to correspond with peak force [Raymond et al., 2009a]. The study provided force and deformation data for each impact, with assumed fracture happening at before 0.5 ms after contact for all PMHS. A summary of the results is presented in Table 2.2.

Table 2.2: Summary of result from Raymond, peak force, deformation at peak force and whether or not fracture occurred. HS/LS indicating high speed or low speed of the impactor.

PMHS ID	**Peak Force [kN]**	**Deformation at Peak Force [mm]**	**Fracture (y/n)**
2426(HS/LS)	5.72/3.02	11.6/8.7	y/n
2427(HS/LS)	9.53/6.35	6.1/4.1	y/y
2904(HS/LS)	5.98/3.17	11.6/9.5	n/n
2908(HS/LS)	4.70/3.66	12.2/8.3	y/n
2939(HS/LS)	4.98/2.48	11.9/8.9	n/n
2965(HS/LS)	6.21/3.55	9.3/6.7	y/n
2978(HS/LS)	3.55/3.38	6.45.2	y/y

2.4.3 Implementation

To begin, the model with the highest impact velocity from the validation catalog was used to determine the range of strain rates occurring during the simulation. This analysis was performed in LS-PrePost by differentiating the strain–time curves. Strain rates were extracted from the elements associated with the impacted regions of the skull. The strain rate magnitude could be used to determine what strain rates to extract from the Bayesian model.

With the rather high velocities, the duration of the impact was very short. As mentioned in section 2.4.2 assumed fracture occurred no later than 0.5 ms after contact was initiated. Because of the short time, the FE solver chosen was the explicit. The explicit solver uses small time steps and ensures quality of

highly dynamic responses.

To evaluate the material properties and the effect of age, different simulations were required. Four categories of simulations were conducted: *aged*, *base*, *scaled* and *pre-project*. The *pre-project* category refers to the material and model configuration used before the start of the project (see Section 2.4.1). In the *base* category, the initial head model combined with material properties for a 50-year-old individual, as described in 2.1.3, was used. Initial model meaning the Viva+ average female and average male depending on the sex of the PMHS. In the *scaled*, the same material properties as in the *base* was used, but the head model was volumetrically scaled to match the mass of each PMHS. The *aged* simulations used the scaled head model, but with material properties corresponding to an 80-year-old individual, also described in 2.1.3. Separate material properties were used for male and female subjects in all cases.

In order for the simulation to produce results similar to those of the experiment, the conservation of momentum had to be taken into consideration. This principle describes how the mass and velocity of two objects influence the outcome of a collision. A scaling was therefore done to the model head to match the head mass of the PMHS. The scaling factor was calculated by the ratio between the PHMS head mass and the model head mass. The scaling was performed by adjusting the head model in the x-, y- and z- directions. Each direction was multiplied by scaling factor. Since the scaling was applied in all three spatial directions, the cube root of the mass ratio was used (see Equation 2.13).

$$\text{Scaling Factor} = \sqrt[3]{\frac{\text{PMHS Mass}}{\text{Head Model Mass}}} \tag{2.13}$$

Scaling the head model altered the placement of the impactor. As described in Section 2.4.2, the experimental impact occurred 25 mm anterior to the external acoustic meatus and 35 mm superior to the Frankfurt plane, slightly behind the temple area. To replicate this placement in the simulation, the distance between the node at the centre of the impactor contact face and the node located directly above the ear canal in the cortical bone was measured in LS-PrePost. The impactor was then repositioned in the x- and z-directions to achieve the distances of 25 mm and 35 mm, respectively.

As noted in Section 2.4.2 the available experimental data consists of force over deformation, with fracture assumed to occur at peak force. Relevant data from the simulation (displacement, time, force, strain) was extracted with the post-processing tool Dynasaur [Schachner et al., 2024], this abled comparison with both to the physical experiments and the risk functions.

After the simulations, deformation was assessed by observing the displacement of the impactor. Because of differences in scaling and impact velocities, the onset of the deformation varied between simulations. Deformation was considered to begin when the force first appeared and to end when the impactor changed direction. This concept was applied in the post-processing of the output from the simulation.

The time at which each simulation reached the deformation observed at experimental peak force (see Table 2.2) was extracted for each category and subject. This time was then plotted against strain over time. By extracting the strain value at this specific time (time for assumed fracture occurrence), the risk of fracture could be evaluated using the appropriate risk function, allowing conclusions to be drawn regarding fracture probability.

3 Results

There were a lot of results from this project, all from correlations, curves and specific values. A summery of the results can be found in the following chapter, some additional results from the project can be found in the Appendix. Furthermore, a general summarization of the data from Wood is provided in Table 3.1.

3.1 Cortical Bone material properties

The results from exploratory data analysis, Bayesian models and the generating of complete stress-strain curves is presented here.

3.1.1 Exploratory Data Analysis

The data extracted from [Wood, 1971] was used to create plots in order to determine what might be correlated with the material defining properties and to acquirer a greater general understanding of the data. Some critical plots and parameters are here included in Figure 3.1 - 3.4 the rest of the plots can be found in Appendix A.

Table 3.1: Summary of the material defining properties in the [Wood, 1971] data.

Property	**Count**	**Mean**	**Std**	**Min**	**25%**	**50%**	**Max**
Young's modulus (GPa)	120	15.42	2.81	10.34	13.55	14.48	22.41
Breaking strain (%)	120	0.64	0.15	0.33	0.54	0.64	1.00
Breaking stress (MPa)	120	81.12	17.00	46.54	68.95	79.29	127.55

In Figure 3.1 the modulus of elasticity as a function of age is shown. Higher strain rate is shown as yellow and lower strain rate as blue/purple. The shape of the dot indicates what part of the bone was used (inner or outer cortical bone). Note the linear correlation between the log_{10} of the strain rate and modulus of elasticity, i.e. gradient in y-direction.

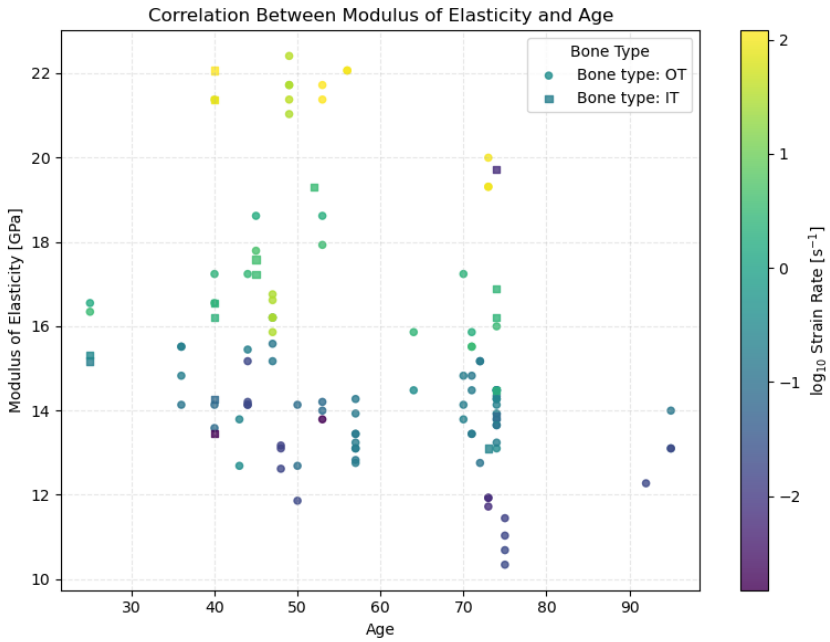

Figure 3.1: Modulus of elasticity plotted against age for the [Wood, 1971] data. The gradient shows log_{10} strain rate.

In Figure 3.2 the modulus of elasticity is plotted against log_{10} strain rate, the gradient shows the age, purple indicating young and yellow older. Note linear behaviour but no clear gradient of ages in the linearity.

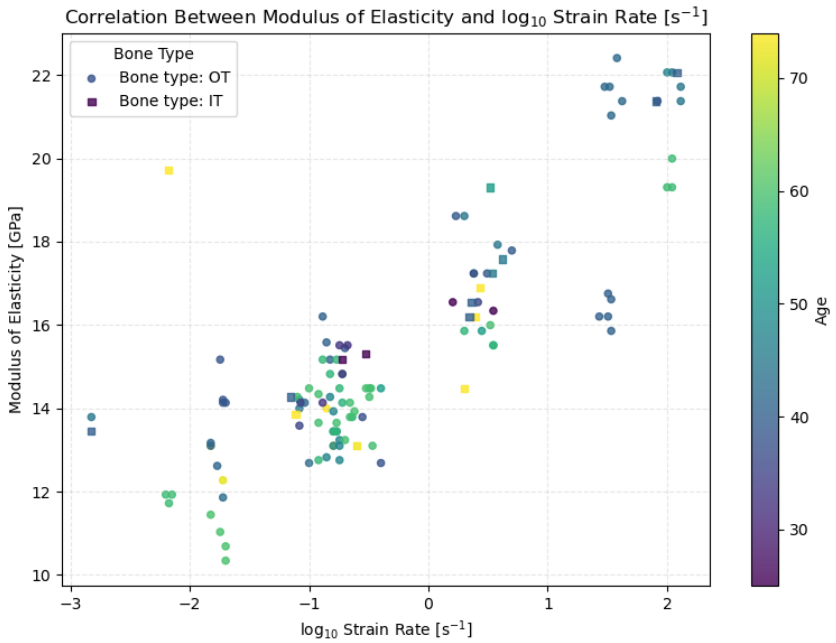

Figure 3.2: Modulus of elasticity plotted against the log_{10} strain rate for the [Wood, 1971] data. The gradient shows age.

In Figure 3.3 and3.4 a linear correlation between breaking strain/ breaking stress and modulus of elasticity is observed. Note the positive correlation in Figure 3.3, negative correlation in Figure 3.4, and how the colours of the dots form a gradient (strain rate).

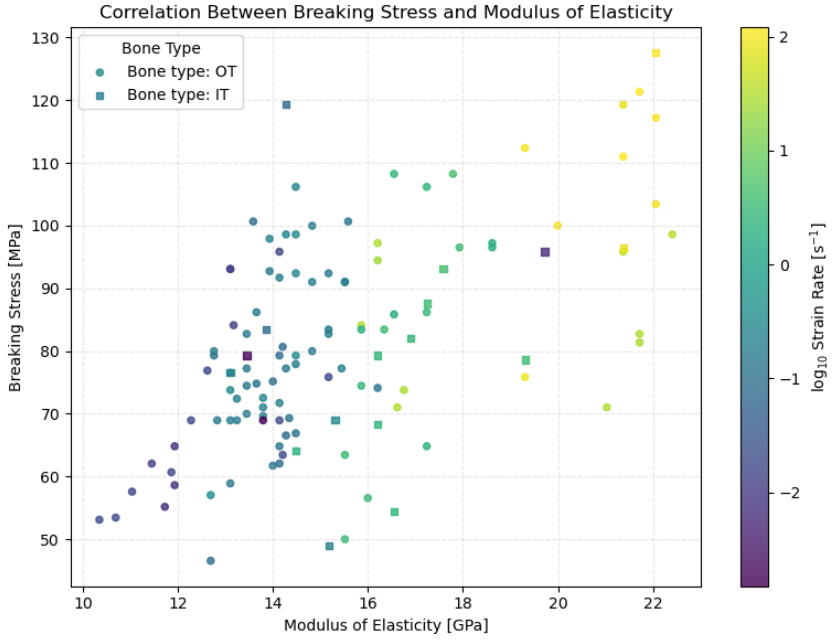

Figure 3.3: Breaking stress plotted against the modulus of elasticity for the [Wood, 1971] data. The gradient shows log_{10} strain rate.

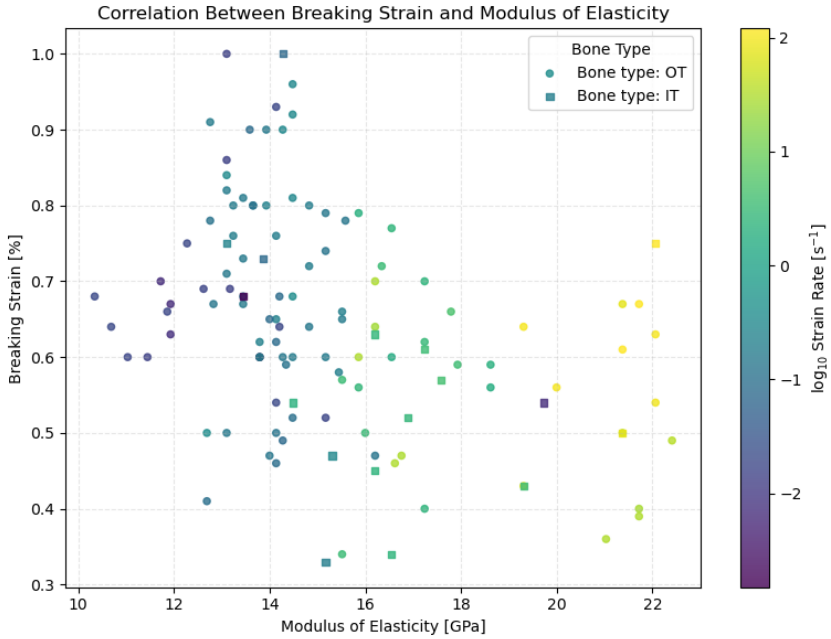

Figure 3.4: Breaking strain plotted against the modulus of elasticity for the [Wood, 1971] data. The gradient shows log_{10} strain rate.

3.1.2 Bayesian models

The results from the Bayesian models are presented here. For each of the three model's the posterior distributions of the intercepts β_0, the slopes β_i and the standard deviations σ_u and σ are presented in Figures 3.5 3.6 3.7. The posteriors for all the u values of each specimen in each model are presented in Appendix Figure B.1 B.2 B.2. Summaries of the posteriors are presented in Tables 3.2 3.4 and 3.6. The probability of each value being either positive ($P(+)$) or negative ($P(-)$) is also presented in Tables 3.2 3.4 and 3.6. Furthermore PSIS-LOO-CV scores are presented for each model in Tables 3.3, 3.5 and 3.7. The names used for the variables of which the posterior distribution of the slopes are given, are defined according to what is described in section2.1.2. The posterior distribution of the standard deviation σ_u is in the Tables and Figures referred to as $1|Speciment2$. The standard deviation σ is referred to as *Sigma* in the Figures and σ in the Tables.

Model predicting modulus of elasticity

Figure 3.5 and Table 3.2 shows that the HDI:s of the posterior distributions for every slope except strain rate varies over zeros. This implies that the degree or the correlation for these variables with modulus of elasticity is uncertain.

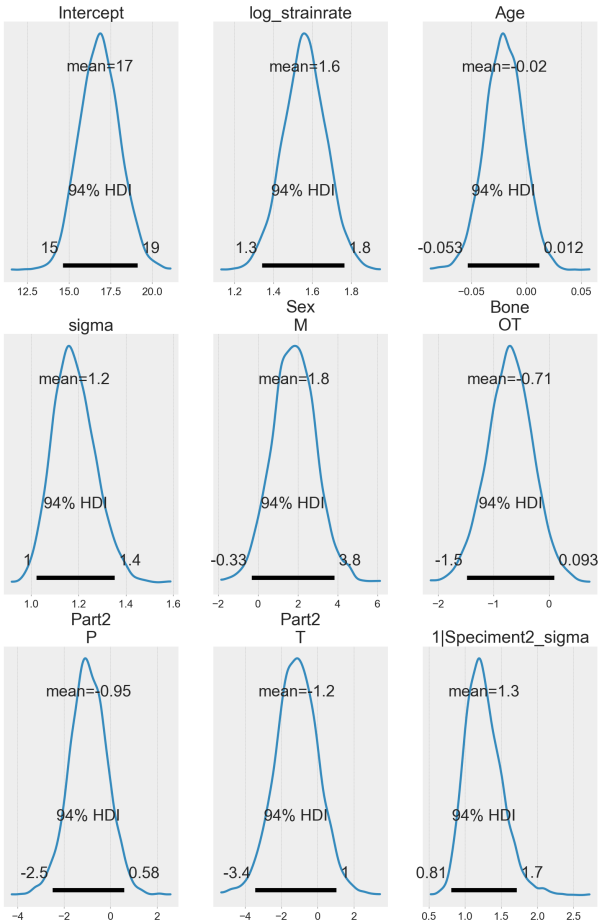

Figure 3.5: Posterior distributions of the slopes, intercepts and standard deviations for the Bayesian model predicting modulus of elasticity.

Table 3.2: Posterior summaries and sign probabilities for model predicting modulus of elasticity.

Parameter	**Mean**	**SD**	**HDI 3%**	**HDI 97%**	$\hat{R}$	**P(+) / P(-)**
σ	1.182	0.089	1.022	1.352	1.00	1.000 / 0.000
Intercept	16.857	1.216	14.635	19.112	1.00	1.000 / 0.000
log strain rate	1.560	0.111	1.341	1.764	1.00	1.000 / 0.000
Age	-0.020	0.018	-0.053	0.012	1.00	0.121 / 0.879
Sex[M]	1.800	1.105	-0.330	3.833	1.00	0.949 / 0.051
Bone[OT]	-0.709	0.414	-1.480	0.093	1.00	0.042 / 0.958
Part2[T]	-1.156	1.194	-3.447	1.038	1.00	0.115 / 0.885
Part2[P]	-0.952	0.818	-2.493	0.582	1.00	0.157 / 0.843
1|Speciment2$_\sigma$	1.258	0.254	0.810	1.713	1.00	1.000 / 0.000

In Table 3.3 the majority of the datapoints used to fit the model predicting modulus of elasticity show good PSIS-LOO-CV scores. There are three points in the data that have an increased effect on the model's performance.

Table 3.3: PSIS-LOO-CV for the Bayesian model predicting modulus of elasticity.

Pareto k range	**Count**	**Percentage (%)**
$(-\infty, 0.7]$ (good)	122	97.6
$(0.7, 1]$ (moderate)	2	1.6
$(1, \infty)$ (problematic)	1	0.8

Model for predicting Breaking Strain

In Figure 3.6 and Table 3.4 the slopes for all the variables' HDI:s ranges over zero, which implies that correlation with the variables and breaking strain is uncertain.

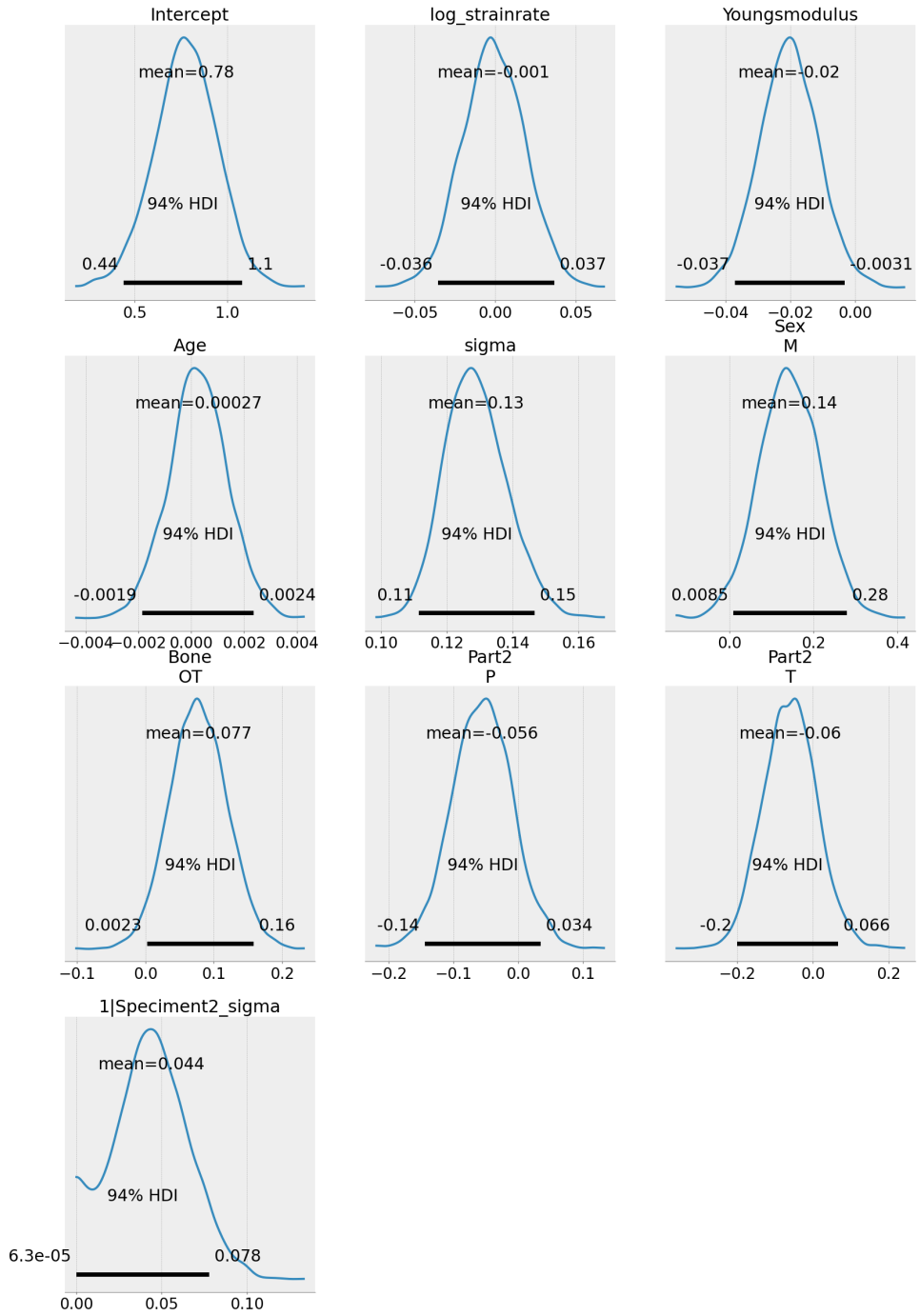

Figure 3.6: Posterior distributions of the lopes, intercepts and standard deviations for the Bayesian model predicting breaking strain.

Table 3.5 shows only one point with a dissatisfactory PSIS-LOO-CV score, implying that the model does not show signs of over fitting.

Table 3.5: PSIS-LOO-CV for Bayesian model predicting breaking strain.

Pareto k range	**Count**	**Percentage (%)**
$(-\infty, 0.7]$ (good)	119	99.2
$(0.7, 1]$ (moderate)	1	0.8
$(1, \infty)$ (problematic)	0	0.0

Table 3.4: Posterior summaries and sign probabilities for model predicting breaking strain.

Parameter	**Mean**	**SD**	**HDI 3%**	**HDI 97%**	$\hat{R}$	**P(+) / P(-)**
σ	0.129	0.009	0.112	0.147	1.00	1.000 / 0.000
Intercept	0.776	0.171	0.439	1.078	1.00	1.000 / 0.000
Youngs modulus	-0.020	0.009	-0.037	-0.003	1.00	0.015 / 0.985
log strain rate	-0.001	0.019	-0.036	0.037	1.00	0.473 / 0.527
Age	0.000	0.001	-0.002	0.002	1.00	0.596 / 0.404
Sex[M]	0.143	0.073	0.009	0.279	1.00	0.973 / 0.027
Bone[OT]	0.077	0.042	0.002	0.158	1.00	0.971 / 0.029
Part2[T vs F]	-0.060	0.072	-0.200	0.066	1.00	0.115 / 0.885
Part2[P vs F]	-0.056	0.047	-0.144	0.034	1.00	0.157 / 0.843
1|Speciment2$_\sigma$	0.044	0.022	0.000	0.078	1.00	1.000 / 0.000

Model for predicting Breaking Stress

Figure 3.7 and Table 3.6 shows every slope except the slope for modulus of elasticity HDI ranges over zero.

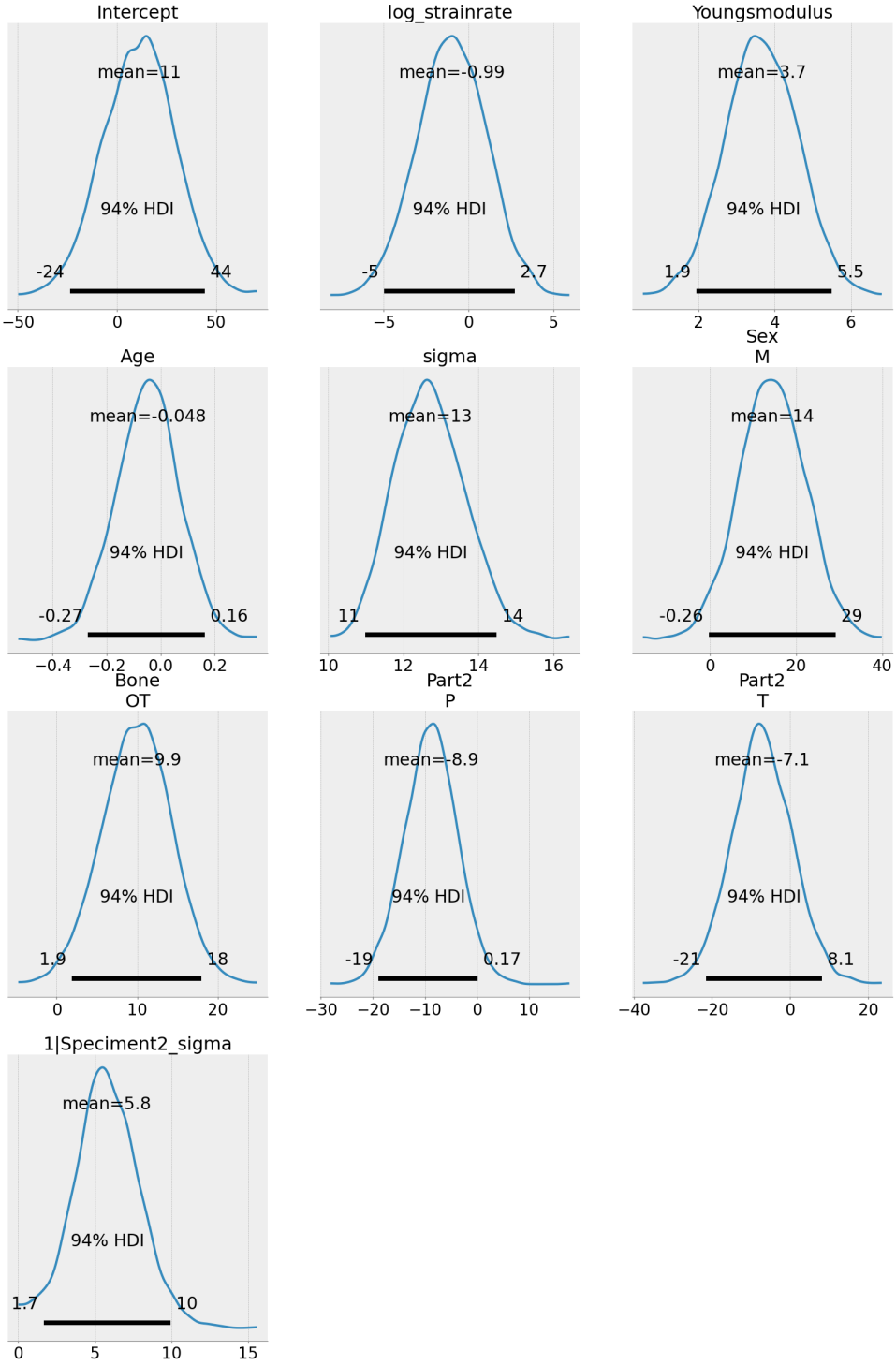

Figure 3.7: Posterior distribution of the slopes, intercepts and standard deviations for the Bayesian model predicting breaking stress.

In Table 3.7 only one point in the PSIS-LOO-CV hows signs of overfitting.

Table 3.6: Posterior summaries and sign probabilities for model predicting breaking stress.

Parameter	**Mean**	**SD**	**HDI 3%**	**HDI 97%**	$\hat{R}$	**P(+) / P(-)**
σ	12.716	0.954	10.977	14.487	1.00	1.000 / 0.000
Intercept	11.262	18.211	-23.739	44.305	1.00	0.731 / 0.269
Youngs modulus	3.655	0.950	1.941	5.483	1.00	1.000 / 0.000
log strain rate	-0.986	2.035	-4.954	2.717	1.00	0.319 / 0.681
Age	-0.048	0.117	-0.269	0.165	1.00	0.340 / 0.660
Sex[M]	14.420	7.818	-0.256	29.252	1.00	0.966 / 0.034
Bone[OT]	9.942	4.284	1.860	17.934	1.00	0.991 / 0.009
Part2[T vs F]	-7.141	7.836	-21.483	8.085	1.00	0.040 / 0.960
Part2[P vs F]	-8.861	5.061	-18.967	0.170	1.00	0.176 / 0.824
1|Speciment2$_\sigma$	5.755	2.133	1.660	9.952	1.00	1.000 / 0.000

Table 3.7: PSIS-LOO-CV for Bayesian model predicting breaking stress.

Pareto k range	**Count**	**Percentage (%)**
$(-\infty, 0.7]$ (good)	119	99.2
$(0.7, 1]$ (moderate)	1	0.8
$(1, \infty)$ (problematic)	0	0.0

3.1.3 Generating complete stress-strain curves

The result of the four stress-strain curves that were generated using the same material defining properties as the stress-strain curves published by [Wood, 1971] is presented in Figure 3.8. All the blue curves are for the higher strain rate and red for the lower. The line style is different depending on if it is the curve from Wood or generated with the second or third degree of polynomial.

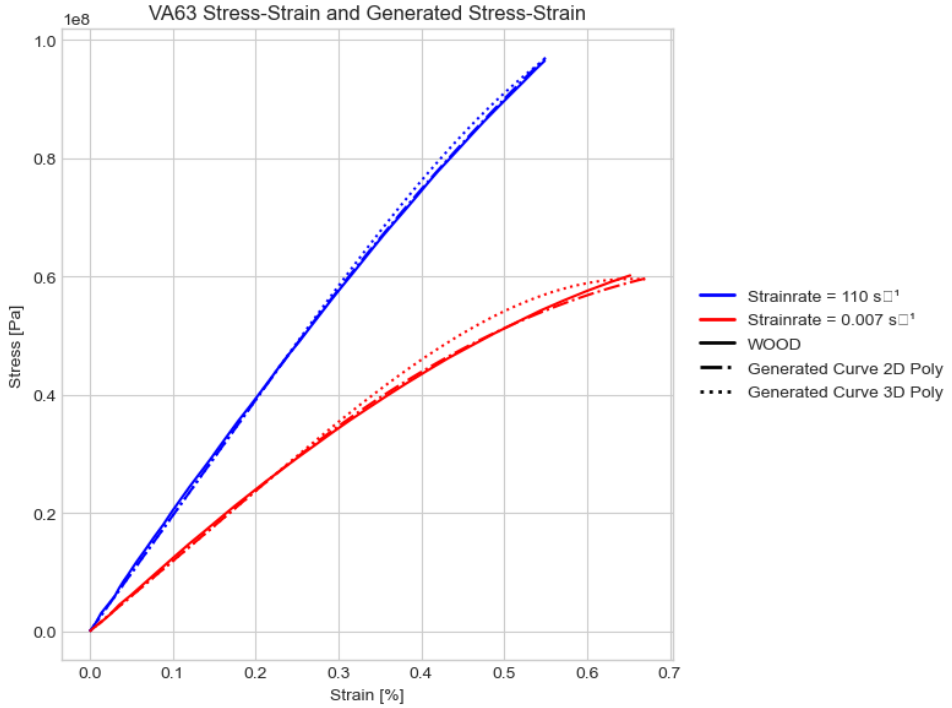

Figure 3.8: VA-63 stress-strain curves from [Wood, 1971] together with the generated curves using the same material defining properties as the published curves.

The root mean square error (RMSE) is presented in Table 3.8 for both the second and the third degree polynomial with two different strain rates, see Equations 2.4 and 2.5. The second degree polynomial showed the lowest RMSE score.

Table 3.8: The RMSE score between the generated curves and the curves from [Wood, 1971].

Model Type	**0.007** $\mathbf{s^{-1}}$	**110** $\mathbf{s^{-1}}$
2D Polynomial	449201	442150
3D Polynomial	1602227	1016429

3.2 Risk functions for Cortical Bone fracture

In the following text the results from the steps for developing the risk function that were presented in Section 2.2. In step 1, where the data was processed, the test data went from 142 test points to 120. In the end of the processing when the mean of the different individuals was calculated the data consisted of 30 tests or data points. In step 2, when COX was used to locate the significant parameters. The Pr value indicated that the only significant parameter was sex, with the value 0.023. The rest of the parameters were not significant, as shown in Table 3.9, a detailed version is shown in Appendix D.1. The parameter Age stands for the age of people, Bone stands for inner or outer cortical. Parameters Part 1 (frontal) and 2 (parietal) the different places on the skull and they are compared with the part 0 that is the temporal. The last parameter is sex, male or female.

Table 3.9: The Pr values from COX regression calculated with the true total breaking strain.

Parameter	**Pr**$(>\|z\|)$
Age	0.166
Bone	0.0872
as.factor(Part)1	0.373
as.factor(Part)2	0.4368
Sex	0.023*

The different significant parameters for the various calculations can be seen in Table 3.10.

Table 3.10: The output for which parameter and the Pr value from the COX regression calculations.

Calculations with...	**Parameter**	**Pr**$(>\|z\|)$
Effective plastic strain	Age	0.0258
Plastic strain	Age	0.0394
True elastic strain	Sex	0.00439
Elastic strain	Sex	0.00439
Total true breaking strain	Sex	0.023
Total breaking strain	Sex	0.023

The results for step 3, where DFBETAS was used identify outliers with the significant parameter can be found in Appendix C.1. Outliers was not taken out from the data. In step 4, the original data points (dataset 2) was plotted together with the different fitted models, see Figure 3.9 and Figure 3.10. The values for the best suitable model is shown in Table 3.11, ta lower value indicating a better fit to the original data (dataset 2).

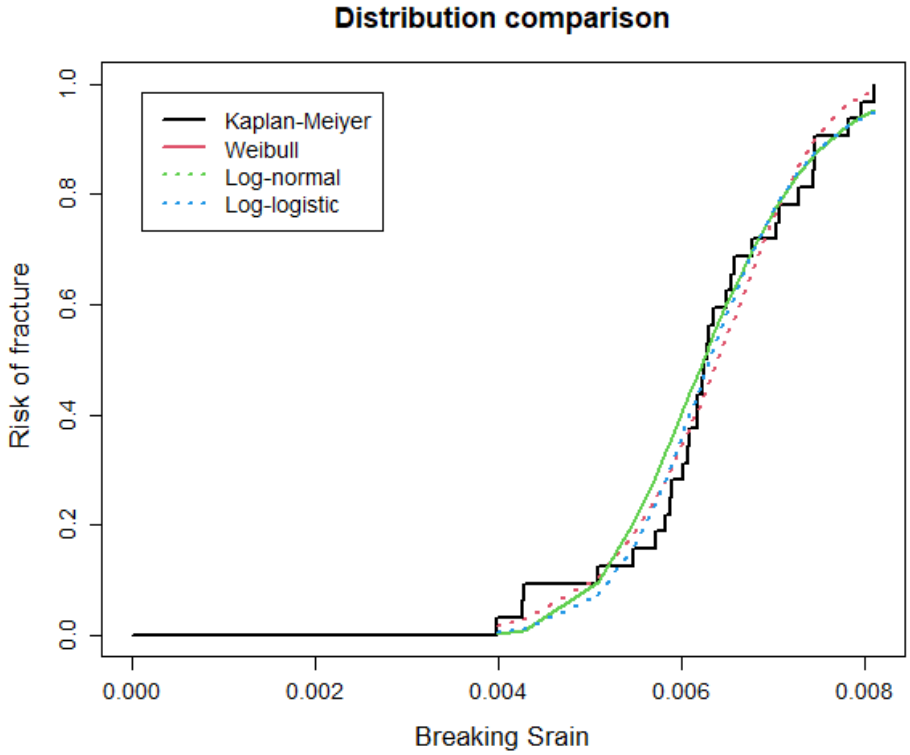

Figure 3.9: The different models and the original data plotted depending on sex.

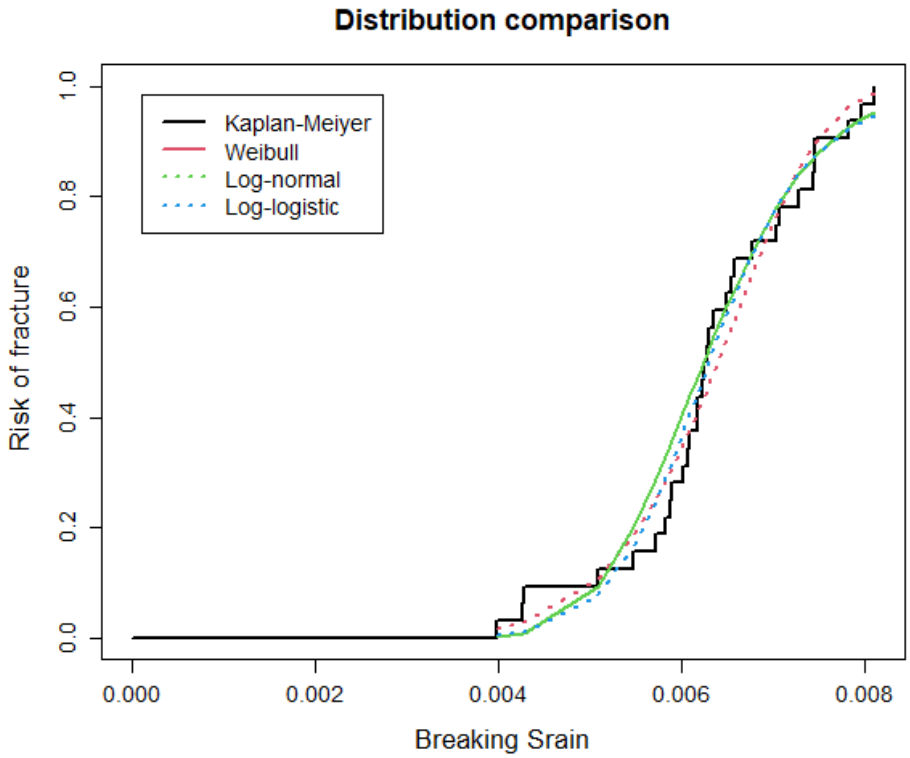

Figure 3.10: The different models and the original data plotted depending on age.

Table 3.11: The AIC score depending on sex or age for the true breaking strain.

Depending on	**Welibill**	**Log normal**	**Log logistic**
Sex	-350.8	-346.8	-347.8
Age	-349.9	-347.2	-347.3

The Weibull distribution received the lowest (best) score for both sex and age dependency (step 5). The equation for the Weibull model is shown in Equation 3.1. The K is the shape factor and the λ is shown in the Equation 3.2, were β_1 is the scale factor and the β_2 is the sex value. For the age depending curve and Equation 3.3 defines λ, where β_2 is the age value. For the parameters see Table 3.12

$$\text{Risk skull fraction} = 1 - e^{-(\frac{\alpha}{e^{\lambda}})^{K}} \tag{3.1}$$

$$\lambda = \beta_1 - \beta_2 \cdot \text{sex} \tag{3.2}$$

$$\lambda = \beta_1 - \beta_2 \cdot \text{age} \tag{3.3}$$

Table 3.12: Parameters for risk calculation for different dependences.

Variable	β_1	β_2	K
Sex	-5.18068	0.195255	2.071135
Age	-5.148565	0.002532	2.053447

The IRC curve based on sex and age is shown in Figure 3.11 and 3.12.

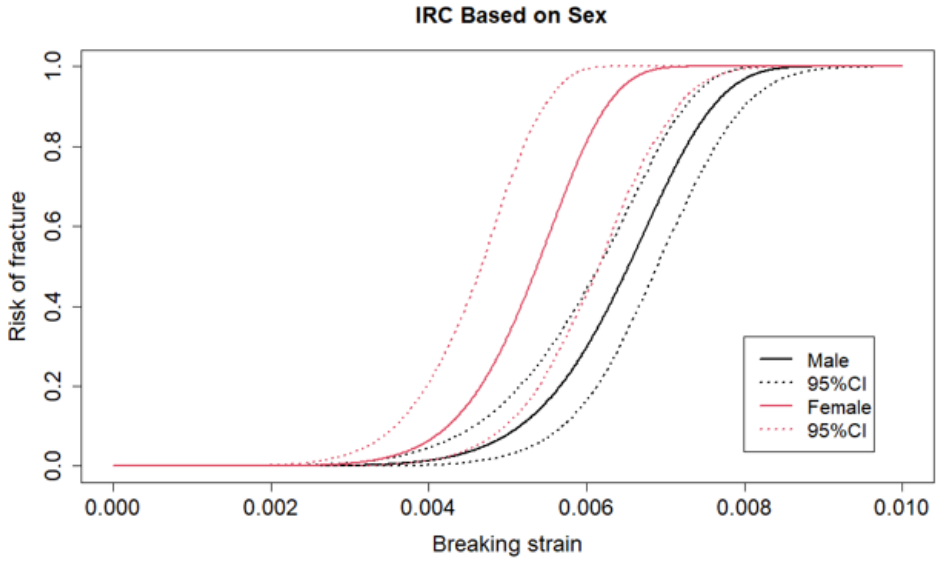

Figure 3.11: IRC curve based on male and female.

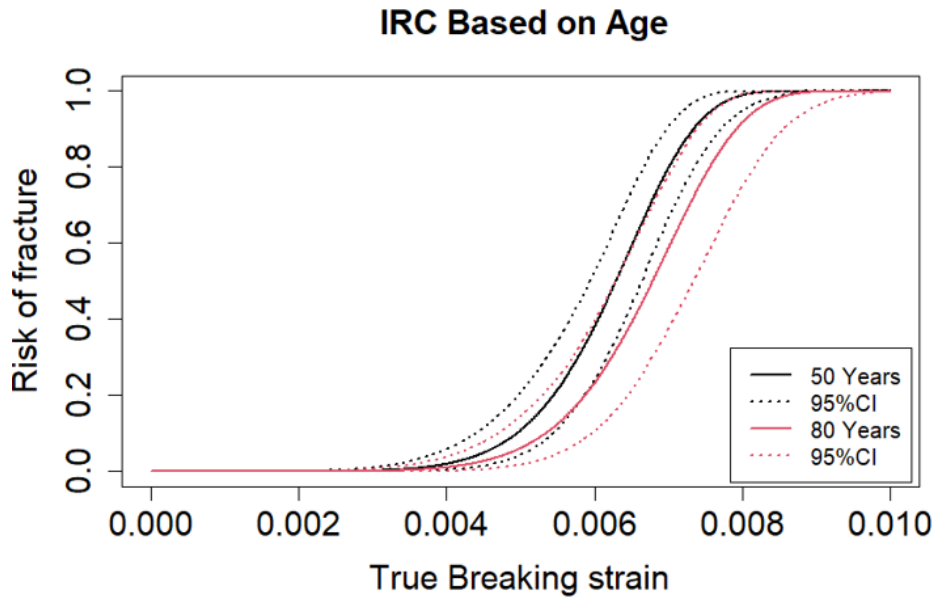

Figure 3.12: IRC curve based on age 50 and 80.

In the last step 7, the result of the upper and lower CI value for the risk curves show that both the curve for the sex dependency and age dependency are of good quality. In the Appendix E all of the result data is shown. In the Table 3.13 a short summary is shown, all the relative CI sizes are within 0.5.

Table 3.13: Quality check- 50-year-old and male.

Injury Criteria	**Risk (%)**	**Estimate**	**Relative CI size**	**Quality Index**
True breaking strain (age as covariate)	5	0.004503	0.249	Good
	25	0.006404	0.112	Good
	50	0.006289	0.116	Good
True breaking strain (sex as covariate)	5	0.0046	0.363	Good
	25	0.0055	0.289	Good
	50	0.0054	0.290	Good

3.3 LS-DYNA implementation of Cortical Bone

Four material cards were created using predicted curves from the regression model on the Wood report.

All material cards contains the same keywords but with different values on the curves. The different strain rates generated different Young's modulus, the material card used the Young's modulus for strain rate 1. The trials with the material card on the dogbone samples were made with the modulus of elasticity for 1, 10 and 100 strain rate. The results for male 80 is shown below in Figure 3.13 and the rest of the results can be found in the Appendix F. Figure 3.13 also contains the results of the Wood study for VA63 to show how strain rates 0.007 and 110 is compared to the results of the predicted curves. In Table **??** you can see what strain rate that occured in the different simulations with the different material cards for the dogbone sample.

Table 3.14: Mean strain rate observed in the simulations for different strain rate curve inputs and demographic groups.

Strain rate Curve Input	**Female Age 50**	**Female Age 80**	**Male Age 50**	**Male Age 80**
1	1.30	0.59	1.35	0.93
10	10.34	9.82	9.83	9.39
100	95.5	100.37	97.44	101.9

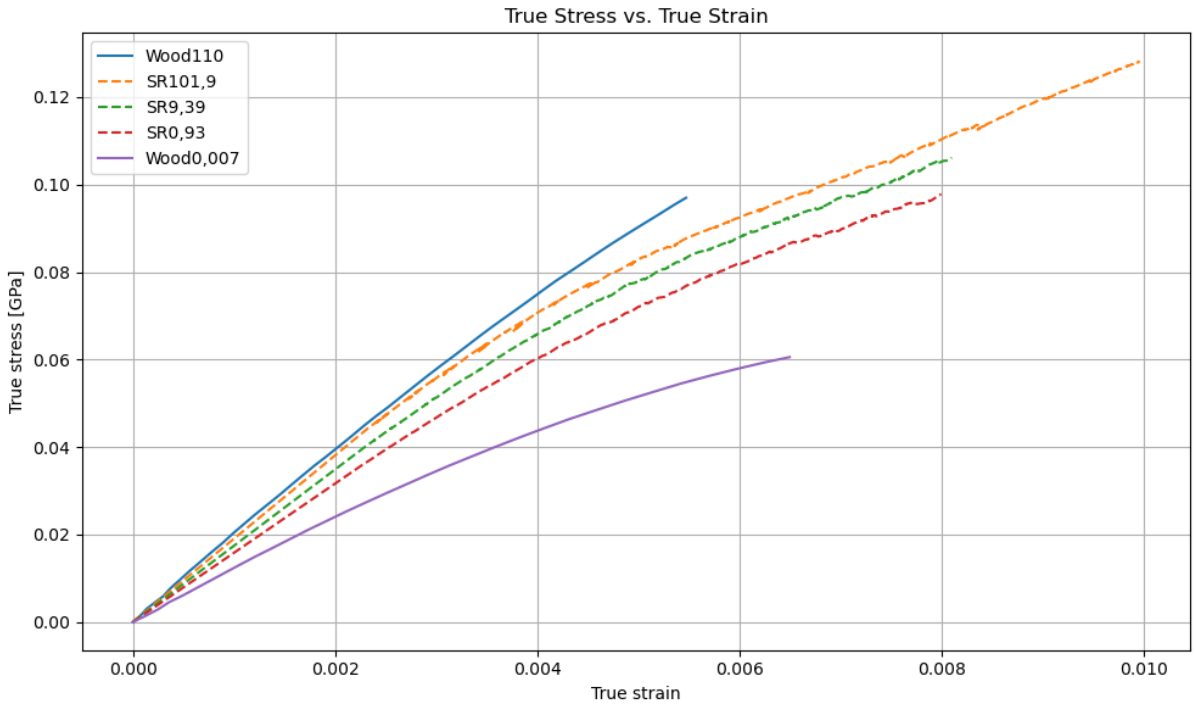

Figure 3.13: Stress-strain curve for a dogbone specimen modeled using the Male 80 material card compared to the Wood result.

In Figure 3.14 the difference with the same strain rate but with different modulus of elasticity is shown, to showcase how MAT024 implements the modulus of elasticity.

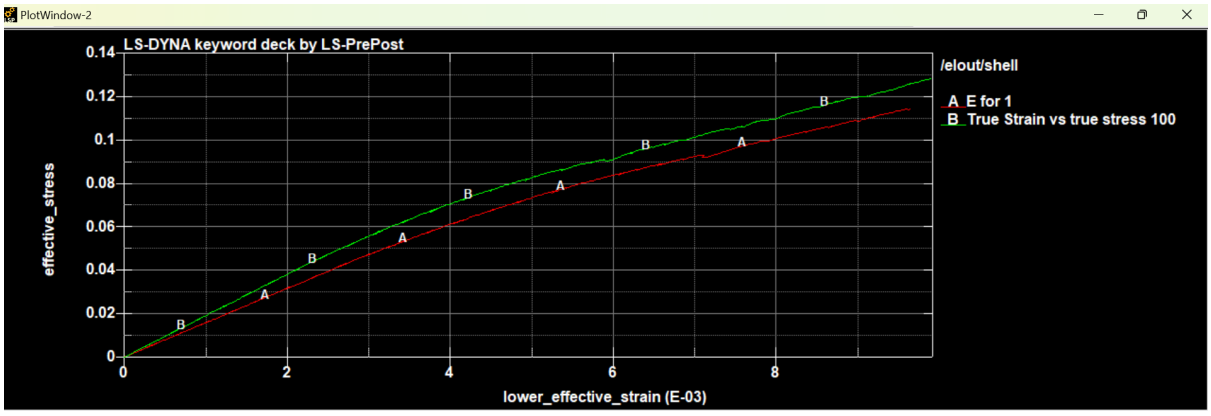

Figure 3.14: B curve is showing strain rate 100 with modulus of elasticity for 100 strain rate and A is showing strain rate 100 with modulus of elasticity for 1 strain rate.

3.4 Head Impact Simulation

The strain rates occurring during the simulation of the impact is shown in Figure 3.15. Note the highest magnitude of the strain rate, 20 -/s $< \dot{\epsilon}_{max} <$ 30 -/s.

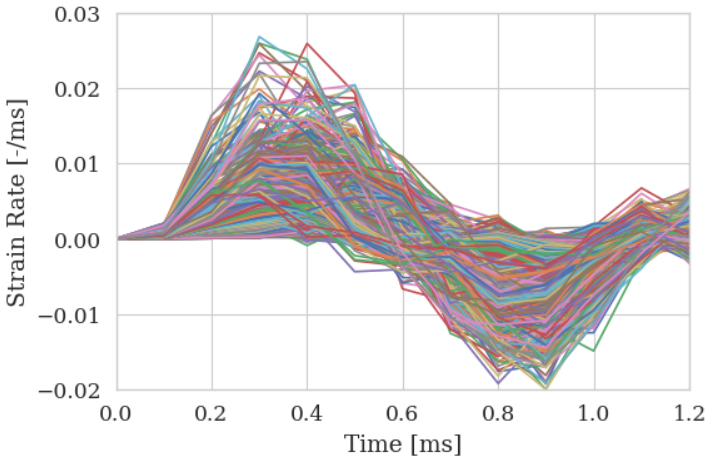

Figure 3.15: Strain rates for elements effected by impact.

The scaling factors for all PMHS are presented in Table 3.15. All of the scaling factors are lower than 1 but no lower than 0.9 compared to the initial model.

Table 3.15: Scaling factors for all PMHS.

PMHS ID	Scaling Factor
2426	0.90351
2904	0.99087
2908	0.96941
2939	0.95047
2965	0.96380
2978	0.93275

The identification of when deformation started resulted in adjustment of the time, force, and other values. In Figure 3.16, an example of the adjustment of force over time for one curve is shown. At most a curve was moved 0.37 ms to account for when the deformation of the head started.

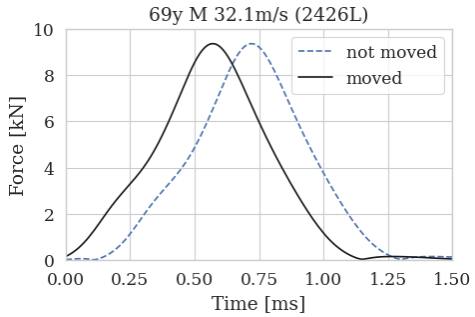

Figure 3.16: Force before and after move.

The deformation for one simulation plotted together with the assumed deformation at fracture and the corresponding time can be seen in Figure 3.17.

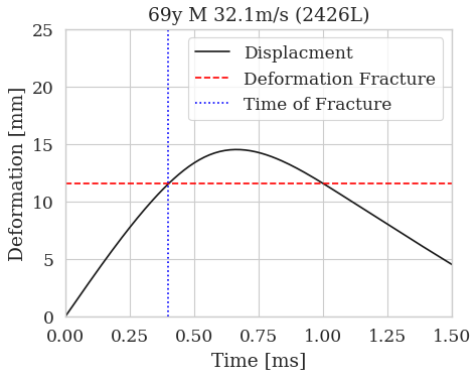

Figure 3.17: Time and deformation for assumed fracture with simulated displacement.

For all categories of simulation, different strains were obtained from the simulation (for definition of the categories see Section 2.4). The result for one of the PMHS in three of the categories can be seen in 3.18. Both 100 percentile and 99th percentile is plotted to evaluate potential extreme element output.

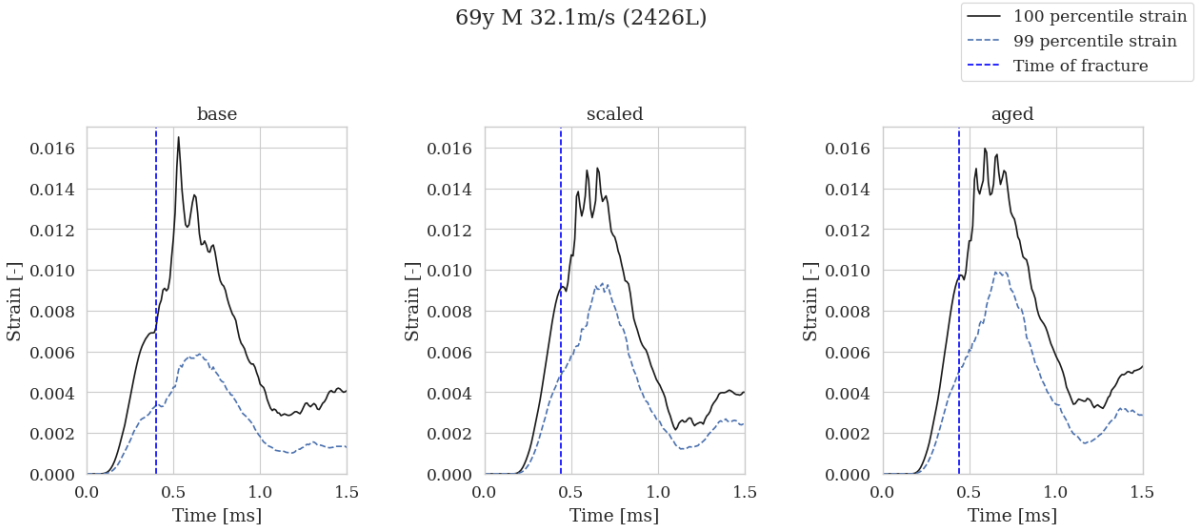

Figure 3.18: Strain at assumed fracture for different categories.

The strain values at assumed fracture for all four categories can be read in Table 3.16 together with information about if fracture occurred in the experiment or not. The strain values at assumed fracture for the 99 percentile strain can be found in Appendix G in Table G.1.

Table 3.16: Maximum strains at predicted fracture time for all PMHS and categories.

PMHS ID	**Velocity [m/s]**	**Fracture (yes/no)**	**Strain [%] pre-project**	**Strain [%] base**	**Strain [%] scaled**	**Strain [%] aged**
2426 (HS/LS)	32.1/22.2	y/n	0.89/0.36	0.90/0.38	0.79/0.54	0.83/0.56
2904 (HS/LS)	31.9/17.3	n/n	0.88/0.09	0.89/0.10	0.88/0.25	0.93/0.23
2908 (HS/LS)	35.1/19.6	y/n	0.93/0.32	1.61/0.37	1.07/0.46	1.14/0.49
2939 (HS/LS)	34.4/16.3	n/n	1.78/0.31	1.61/0.32	0.99/0.08	1.07/0.09
2965 (HS/LS)	35.2/18.0	y/n	0.73/0.29	0.82/0.34	0.44/0.38	0.45/0.40
2978 (HS/LS)	32.4/19.5	y/y	0.40/0.25	0.43/0.27	0.17/0.01	0.17/0.01

As mentioned in Section 2.4.2 specimen 2427 was excluded in the results. The simulation was done for specimen 2427, results can be found in Appendix H in the Tables H.1-H.3.

In Table 3.17 the risk of fracture is specified together with whether or not fracture occurred in the experiment. HS meaning high speed and LS low speed. The risk of fracture for the 99th percentile strains can be found in Appendix G in the Table G.2.

Table 3.17: Risk of Fracture for all subjects, calculated with variables depending on age (50 or 80 years).

PMHS ID	**Fracture in experiment (yes/no)**	**Risk of Fracture scaled [%]**	**Risk of Fracture aged [%]**
2426 (HS/LS)	y/n	91.51/66.64	95.75/75.55
2904 (HS/LS)	n/n	95.16/21.06	98.09/20.15
2908 (HS/LS)	y/n	98.96/55.88	99.77/66.39
2939 (HS/LS)	n/n	97.97/2.44	99.52/3.40
2965 (HS/LS)	y/n	51.25/42.55	58.71/50.28
2978 (HS/LS)	y/y	9.36/0.01	11.21/0.01

4 Discussion

This section analyses and interprets the results presented in the previous chapters, focusing on the implications of ageing on cranial material properties and the accuracy of simulating head impacts. The comparison between simulation outcomes and experimental data provides insight into the limitations and strengths of the current modelling approach.

4.1 Cortical Bone material properties

As noted by Wood in his original study [Wood, 1971], age did not appear to be correlated with breaking strain and stress, though a weak correlation with modulus of elasticity was observed. In this study, a more comprehensive analysis using Bayesian statistical methods was conducted to explore these relationships further.

Given the project's primary goal of examining how age affects cranial bone behaviour, the initial scatter plot of modulus of elasticity versus age (Figure 3.1) raised concerns. The data showed considerable spread and only a weak negative linear trend. However, this variability can largely be attributed to the influence of strain rate, which differs across samples. Specifically, higher strain rates were associated with higher modulus of elasticity values, suggesting that strain rate plays a dominant role in modulating modulus of elasticity. Visible by the colour gradient of the scatter plot.

Despite the weak direct correlations between age and breaking strain or stress, these relationships were included in the Bayesian models to asses whether any deeper patterns might emerge. The scatter plot in Figure 3.2 confirms a strong linear correlation between modulus of elasticity and log_{10} strain rate. Additional plots, (see Appendix A) reveal that the breaking strain and stress also correlates with strain rate to a certain degree. Moreover, both breaking strain and stress exhibited correlations with modulus of elasticity (Figure 3.4 and 3.3), prompting its inclusion as a predictor variable in the Bayesian models.

The posterior distributions for the model predicting modulus of elasticity (Figure 3.5) reinforces the earlier observation: there is a strong linear correlation with log_{10} strain rate, evidenced by a narrow 94% HDI between 1.3 and 1.8. The correlation with age, however, remains inconclusive. Its posterior distribution spans zero, indicating that the correlation could be either positive or negative, although the mean suggests a weak negative trend (3.2). There remains a 12.1% probability that the correlation with age is actually positive.

Regarding breaking strain and stress, the Bayesian models showed similarly inconclusive results. The posterior for age-breaking strain relationship shows a nearly neutral trend with a 59.6% probability of being positive (Table 3.4), while the correlation with breaking stress is more likely negative, but only with a 66.0% probability. These wide distributions highlights the limitations of the original dataset in reliably determining the influence of age.

However, a more consistent and interpretable pattern emerged when considering indirect correlations. Modulus of elasticity, which is more confidently predicted from strain rate and age, showed a significant negative correlation with breaking strain (98.5% certainty) and a significant positive correlation with breaking stress. This suggests that as modulus decrease breaking strain may increase and breaking stress decrease. Though this pathway is indirect, it aligns with and supports the weaker age correlations, providing a more nuanced view of how ageing could influence bone response.

It is important to note that, for curve generation, only the mean correlations from the Bayesian posterior distributions were used to derive material properties. These properties were then applied to construct stress-strain curves, which was implemented in LS-DYNA. Thus, while the Bayesian analysis offered richer insights, this information was not fully used in this project.

The limitations of the Wood dataset should also be acknowledged. What can be concluded using the Bayesian analysis is that the data published by [Wood, 1971] is insufficient in determining if there is any correlation between age and the breaking stress/strain of the material. It includes multiple samples from a limited number of individuals, increasing the potential influence of outliers.

Furthermore, the experimental equipment used by [Wood, 1971] is old and can be assumed to have a lower

precision compared to modern equipment. The spread in the data which can not be explained by any of the fixed variables or the spread caused by variation between specimens is expressed as ϵ_i in Equation 2.2. ϵ_i is assumed to be normally distributed with the standard deviation of σ, see Equation 2.3. The posterior distribution of σ consequently conveys how much variation is caused by unknown factors, such as imprecise equipment. The σ for the model predicting modulus of elasticity has a mean of 1.2 GPa and and a 94% HDI between 1 GPa and 1.4 GPa (see Figure 3.5 and Table 3.2). It is therefore likely that there is around 1.2 GPa standard deviation (corresponding to a coefficient of variation $\frac{\sigma}{Mean}$ of 8%) for modulus of elasticity not explained by either the variables of the model or the random variation between different specimen. The σ for the model predicting breaking strain has a mean of 0.13% (corresponding to a coefficient of variation of 20%) with a 94% HDI of 0.11% to 0.15% (see Figure 3.6 and Table 3.4). The higher value of the coefficient of variation of the σ for breaking strain suggests that there is more unexplained variation in the breaking strain compared to modulus of elasticity. The σ of the model predicting breaking stress has a mean of 13 MPa (corresponding to a coefficient of variation of 16%) with a 94% HDI of 11 MPa to 14 Mpa (see Figure 3.7 and Table 3.6).

It is impossible to say without further research what causes the variation. It can not be time post-mortem, random variation between individuals or other variables specific to certain individuals. The variation between individuals fall under the σ_u standard deviation, see $u_{j[i]}$ in Equation 2.2. The posterior distributions of σ_u are presented under the name *speciment2_sigma* in Figures 3.5, 3.6, 3.7 and have significantly lower means than σ. It is possible that some of the variation described using σ is caused by the imprecision in the experimental equipment used by [Wood, 1971]. It is also possible that the unexplained variation is caused by random variation of material properties within the skull itself. The fact that the corresponding coefficient of variation for σ is higher for breaking strain and stress compared to modulus of elasticity suggests that the cause is not random deviation within the skull. There are no reasons for such random variation to be larger for breaking strain and stress compared to modulus of elasticity, it is rather more likely that the experimental equipment is more imprecise measuring breaking strain and stress. A new experimental study of the skull bone material would be useful to increase the certainty of the effects age has on the material properties of skull bone.

The models PSIS-LOO-CV showed that some data points influenced the performance of the model significantly, see Table 3.3, 3.5, 3.7. Most likely caused by outliers in the data. If these outliers are due to imprecision in the experiment or actual random variation is impossible to determine.

The function used to generate complete material curves (Equation 2.4) was selected due its low RMSE compared to Wood's experimental curves and its favourable mathematical behaviour. Unlike other curve forms, it is impossible for a curve to end with a negative slope, which would otherwise cause technical issues in LS-DYNA simulations.

4.2 Risk function for Cortical Bone fracture

The ISO standard [International Organization for Standardization [ISO], 2014] for creation of risk functions for car crash simulations was not followed exactly in this project. Because this project is not about car crash simulation but about how the simulation program do not have material cards for an aged skull. The first four steps from Section 1.3.2 are combined in the first step in Section 2.2. In the Wood data all the data points are representing fracture and the fractures were caused the same way. The steps 2 - 4 from Section 1.3.2 did not fit the work with the Wood data and were therefore combined with the first step in Section 2.2.

There are many things that affects the results of the risk functions. One of the most significant is the Wood data in it self. In the experiments, many of the variables varies from the different tests that were performed. For example, the strain rate vary between 0.005 [%/sec] to 130 [%/sec]. These variations make it harder to find patterns and clear trends in the data. When the data was plotted in different configurations it was shown that the Wood data did not have clear trends. That is why the mean was taken to try to prevent outliers that were hidden because of the variations in varietals.

The variation between different individuals is significant. This can entail that some of test data deviates from the norm, stronger or weaker skulls. With as few individuals as 30, between the ages of 25 and 95, the outliers become more difficult to identify since the norm is not known. Wood made many tests on samples from the same skull, potentially causing an outlier to be more prominent than if only one

test was done. The number of samples and performing Wood's test with variating the variables can be significant reasons as to why the risk function result is not that dependent on age.

In Table 3.10 it is shown that sex is more significant than age for the risk function. The reason for this is unknown. One of the contributing causes may be that there is fewer females than men, and therefore more important data for the algorithm. In the data from Wood only three individuals were females. It could also depend on, as mention above, that the Wood data is not optimal for this project. In Appendix C in Figure C.1 the right picture shows the data from the different individuals mean data represented as columns. The fourth bar is an outlier and the second bar is almost an outlier, these two individuals are females. If those two are taken out of the dataset there would only be one female left, and this would probably affect the result. Therefore, the outliers are still included in the dataset.

In step 2) the age was calculated to not be significant but the risk curve shown in Figure 3.12 shows a small dependency. Even though it is not that significant, a difference is still shown between a younger and older individual. The quality check in Appendix E shows that it still is a good curve. Woods data does not necessarily show all reasons that could cause change in the skull and those are therefore not taken into account. In combination with the result from the risk curve with dependence on age, Figure 3.12, it shows that older people withstand more pressure than younger. Could be that an older skull deform more than a young skull.

Figure 3.9 and 3.10 shows the distribution comparison with the different significant variables, sex and age. They are almost the exact same distribution, but the estimated models differs from each other. Even though, according to Table D.1 in Appendix D, age should not be significant for the risk function, both curves in the quality check results in good curves. Maybe with another dataset than Wood, bigger differences would appear because of all the reasons already presented about the Wood data and its limitations.

In conclusion there is a connection that data selection can be one of the more contributing problems for the project's risk function. With more time additional data to supplement and introduce as a base for the risk functions could have been added. If that data also shows that older skulls can endure higher pressure than younger then confidence of the Wood data increases. If not, more studies are needed to find why different data show different results. There could be various reasons why the results differ between different tests. Some of the reasons may be how the tests are conducted or how many skulls are in the test and which from what kind of subjects, female, male, young or older.

4.3 LS-DYNA implementation of Cortical Bone

The material calibration part has a lot of variables that could affect the results and it is difficult to confirm if it is correct since there is no other research with generated curves from a material prediction to compare with.

Aleksandra Krusper, the scientist that made the material card for the current VIVA+ model, had a presentation about the thought process when working with the material card and shared her results. The difference in this work compared to Krusper is that her curves were defined for exactly the Wood curve of sample VA74 [Wood, 1971], while this work is trying to predict the curves for different ages. With her material card as a template, the necessary parameters were changed but the rest were kept the same.

The predicted curves had less stress than the results Wood had. This can be seen in 3.13 where the Wood result for strain rate 0.007 and 110 are shown with the predicted curves for M80. The lower strain rate of 0.007 is far more off than the rest. This is because the strain rate gives logarithmic results, lower strain rate causes bigger difference. That is why 0.007 in strain rate differs more from 1 in strain rate than 1 differs from 10 for example. The reason that there are no results of the lower strain rate in this project is simply because of how the strain rate is calculated with the displacement and time. The time is the variable that is changing, and to increase the time to get a strain rate of 0.01 would make the simulation take too long to run. Since the results on the dogbone sample simulation for the higher strain rates were a success with the generated curves, the lower strain rate curves were assumed to be correct. With that in mind, the curves for 0.01 and 0.1 were included in the material card.

Something that could be done about the time aspect is to change the FEM solvers from explicit to implicit. This is something interesting and takes more experience since it's easy to make the function unstable in explicit Euler calculations but could potentially make the results better for lower strain rates. The other option might be to use MAT187L or some other material parameters that uses different modules of elasticity into consideration in a single simulation.

The final simulations used MAT024 as material definition, this was not supposed to be the final results but with the lack of time and experience in LS-DYNA, MAT024 was the only material keyword where results were able to be produced. As mentioned in the method, in Figure 3.14 you can clearly see that the input modulus of elasticity does change how the curves behave even though it's supposed to be the same material card. To improve these results for the material card there would have to be some kind of implementation of the modulus of elasticity as a function. This is how MAT187L works, it consider the material more like a plastic instead of a metal. This give the elastic part before the yield point a function based linearity. Instead of defining a modulus of elasticity for the whole simulation, you define it for each curve. MAT187L was the keyword that were supposed to be used, but since Krusper used MAT024 the files that were shared used MAT024. MAT024 was therefore the material keyword that got the first set of results and there were no time to get MAT187L running.

The material cards had to be ran 3 times for each card with 3 different modulus of elasticity because MAT024 were used. Even though MAT024 is the worse choice, it does still work considerably well and were able to fit the predicted curves good enough in the simulation when compared to the Wood data. In the Appendix F, the rest of the results are shown for each material card on the dogbone sample.

The results clearly shows that the bigger the modulus of elasticity and strain rate are, the higher the stress gets. It can also be seen that the lower the age, the higher the stress goes up to. This is because a lower age provided a higher modulus of elasticity, which further shows the conclusion. You can also see that male gets higher stress values than the female and this is also because males had higher modulus of elasticity. This information says that with the same dogbone sample, where the material card is changed to different age and sex between the simulations, there is a difference in the maximum stresses that occurs in the simulations.

One of the bigger problems with the dogbone results and the material card is that it does not show in the simulation if the dogbone breaks or not. The only thing that could be taken out is how the curves behave during the simulation.

Since MAT024 only uses one modulus of elasticity per material card, the group decided to use the value of the modulus when the strain rate was 1 for each age and sex. This was because the strain rate of 1 was the most reasonable strain rate to occur in the simulation on the HBM. Since the strain rate changes the stress/strain curves on a logarithmic scale it seemed reasonable to take one of the lower strain rate modulus of elasticity. Also, in Figure 3.15 which shows the occurring strain rates on the HBM, you can see that most of the strain rates that occurs are between 0 and 10 with a maximum of around 30. This is also why the curves are based on strain rate 0.01, 0.1, 1, 10 and 100. The material card had to be able to read strain rates over 30 and close to 0, hence those curves.

Another problem with the results is how the strain rate for the experiment were calculated. Trial and error was the only option while working with displacement and time to find the correct strain rates. There should be another option on how to better and automatically find the wanted strain rate but none were found with this time span. Since Krusper showed that she found the correct strain rate with trial and error in her her study as well, the group felt confident about using this method as well. This method meant that it was hard to find the exact strain rate that were looked for since the simulation had to be remade if the strain rate was to off.

The graphs for the material card on the dogbone samples aimed to show how the curve would behave exactly at the strain rate used to create each curve. This became almost impossible even though the group settled with strain rates that were close enough. Strain rate were one of the big dependencies that were found on the prediction of the curves. Therefore, this might have an impact to someone who would try to use the curves from this work to validate dogbone samples for strain rate 1, 10 and 100. That is why the curves are presented with the exact strain rate that occurred instead.

The stress and strain curves of the simulation for the dogbone sample does not have anything to do with the results for the HBM. The results of the dogbone sample are there to show how the dogbone sample results differ depending on the material card and strain rates. The results could give a picture of how the results should differ for the viva+ model but are not to be taken as a direct translation. The conditions in the simulation is what decides how the material card are implemented and in Figure 3.15 you can see all the different strain rates that occurrs in the different elements. As discussed before, this then would affect the modulus of elasticity and with that, an appropriate curve from the material card are implemented. You can also see that most of the element has relatively low strain rates. This meant that the material card had to have curves for very small strain rates even if there were no time to verify them since it would have taken to long.

4.4 Head Impact Simulation

All PMHS used in the study had a lower head mass compared to the baseline model (both female and male), as shown by the scaling factors in Table 3.15. The reason for this lower mass is unclear. As mentioned in subsection 2.4.1 the model is based on a 50th percentile human. Based on that, the PMHS should ideally include individuals both above and below this benchmark. However, since only six PMHS were included in the experiment, it is plausible that the samples do not accurately reflect the general population distribution.

Table 3.16 shows the strain values across the different model categories. The most significant difference appears when comparing the unscaled and scaled models. For instance, in specimen 2939R, the difference between the aged and scaled categories is only 0.0008, whereas the difference between the base and scaled is 0.0062. This highlights the importance of matching model's head mass to that of the PMHS head mass and supports the decision to apply head mass scaling. Other anatomical factors, such as skull and scalp thickness, also varied among the PMHS and could significantly impact the results. For example, the scalp thickness ranged from 5 mm to 16 mm, and for the skull thickness 3.5 mm to 6.3 mm (Table 2.1). It is reasonable to assume that increasing the lowest value by 80% or 200% could substantially influence the outcome.

The difference between the aged and the scaled data suggests that older individuals experience higher strain under the identical impact conditions. Assuming fracture occurs at a consistent strain threshold, this implies an increased fracture risk in the elderly. This further supported by the calculated fracture risks for the strain values (Table 3.17). In nearly all cases, the aged model shows a higher risk of fracture than the scaled model, i.e. 80 years shows slightly higher risk of fracture than 50 years.

However, the accuracy of the fracture prediction is limited. For example, specimen 2939 shows a 99.52 % risk of fracture in the simulation, yet no fracture occurred in the experiment. Conversely, for specimen 2978, the simulation predicts a fracture risk of only 0.0%, but a fracture was observed experimentally. These discrepancies may stem from assumptions made in the simulation - such as defining fracture onset at a specific deformation. Another source of uncertainty is the limited sample size. With only seven PMHS, and just six considered to yield reliable data, the findings may not be generalizable to a broader population.

Despite these limitations, there are results that align reasonably well with the experimental outcomes reported by Raymond. For example, specimen 2908 and 2965, both closer in age to 80 than 50, show fracture risk predictions in the aged model that are more consistent with the experimental results.

In conclusion of this project, the predicting of risk of fracture is a bit unstable, the cause of this is unclear as many possible weak points has been identified. Because of this further work is needed to establish a better material of an ageing head.

4.5 Future Work

As previously mentioned in Section 4, many weak points and ideas about additional relevant data has been identified. In this subsection the possible changes and additions are summarized.

The variation in skull and scalp thickness among the subjects were considerable, as discussed in Section 4.4. To more accurately replicate the Raymond study, these anatomical parameters should incorporated

into the model. Moreover, assessing the correlation between age and skull/scalp thickness would enable a more realistic simulation of head characteristics for individuals of specific ages.

This project compared two distinct age groups. For future work, it would be valuable to develop a function that generates material property curves with age as a parameter, allowing for age-specific material modelling. A comparable approach is already implemented in the HBM for certain parameters related to sex. Additionally, the material model could benefit from inclusion of more stress-strain curves at various strain rates, leading to greater accuracy. Currently, the FE software interpolates between the limited number of input curves, which may reduce precision.

The data used for the Bayesian statistic model and the fracture risk function had several limitations. Notably, only three females subjects were included in the dataset, potentially leading to biased or unrepresentative outcomes. Furthermore, the original experiment was conducted in 1969. Since then, significant advances have been made in experimental techniques and data collection. Incorporating more recent and comprehensive datasets would enhance the robustness of the model.

Additionally, it is important to note that Wood's conducted tensile tests, whereas the cranial bone is more frequently subjected to compressive rather than tensile forces during impacts. Therefore, further research into the compressive behaviour of the cranial bone would be beneficial for refining HBMs. To improve accuracy, a similar project should be done for the trabecular bone to determine the the impact age has one the material properties. Wood's study primarily focused on the cortical bone, with minimal data collected on trabecular bone, leaving a gap in understanding that needs to be addressed in future studies.

For the material implementaion, MAT187L should be used if similiar tests were to be done again. This is discussed a bit in the discussion 4 and why this would be much better. MAT187L could potentially be faster in the simulations for low strain rate as well and could therefore provide results for a dogbone sample for the low strain rates.

5 Acknowledgements

We'd like to thank a few people for their contribution to the project and support along the way. Firstly, thanks to our supervisor Jobin John for his support and ambition for the project. Another thanks to our examinator Johan Davidsson for introducing the subject of traumatic brain injuries and risk curves, as well as the support in producing risk functions. Another major contributor to the risk functions is Yash Niranjan Poojary, thank you for your support and quick answers to questions. Lastly but not least, Aleksandra Krusper thank you for the help with the material specific questions in LS-DYNA and with the help to make the simulations work when the group were struggling. Also thank you for providing information from your own work so that we had some files and results to start from.

References

[Adanty et al., 2021] Adanty, K., Rabey, K. N., Doschak, M. R., Bhagavathula, K. B., Hogan, J. D., Romanyk, D. L., Adeeb, S., Ouellet, S., Plaisted, T. A., Satapathy, S. S., and Dennison, C. R. (July 2021). Cortical and trabecular morphometric properties of the human calvarium. *Bone*, 148. https://doi.org/10.1016/j.bone.2021.115931.

[Ansys, 2025] Ansys, I. (January 2025). *Ansys LS-DYNA*. Retrieved 6 May, 2025, https://www.ansys.com/products/structures/ansys-ls-dyna.

[ArviZ Developers, 2025] ArviZ Developers (2025). *ArviZ: Exploratory analysis of Bayesian models*. Retrieved 2 May, 2025, https://www.arviz.org/.

[Bambi Developers, 2025] Bambi Developers (2025). *Bambi: Bayesian model-building interface in Python*. Retrieved 2 May, 2025, https://bambinos.github.io/bambi/.

[Boskey and Coleman, 2010] Boskey, A. L. and Coleman, R. (2010). Aging and bone. *Journal of Dental Research*, 89(12):1333–1348. https://doi.org/10.1177/0022034510377791.

[Davidson-Pilon, nd] Davidson-Pilon, C. (n.d.). Estimating univariate models. https://lifelines.readthedocs.io/en/latest/Survival%20analysis%20with%20lifelines.html.

[DYNAmore, nd] DYNAmore (n.d.). *"DYNAmore Human Body Model"*. Retrieved 11 February, 2025, https://www.dynamore.de/en/products/models/dynamore-human-body-model.

[DYNAmore GmbH, 2002] DYNAmore GmbH (May, 2002). *From engineering to true strain, true stress*. Retrieved 1 April, 2025, https://www.dynasupport.com/howtos/material/from-engineering-to-true-strain-true-stress.

[DYNAmore GmbH, 2020] DYNAmore GmbH (May 29, 2020). *DYNAmore Express: Good old *MAT_024 - A review of LS-DYNA's most popular material model*. Retrieved 15 April, 2025, https://www.dynamore.se/en/downloads/presentations/dokumente/dynamore-express-good-old-mat_024-a-review-of-ls-dyna2019s-most-popular-material-model.

[Edinburgh et al., 2023] Edinburgh, T., Ercole, A., and Eglen, S. (2023). Bayesian model selection for multilevel models using integrated likelihoods. *PLOS One*, 18(2):e0280046. https://doi.org/10.1371/journal.pone.0280046.

[Global Human Body Models Consortium, nd] Global Human Body Models Consortium (n.d.). *GHBMC*. Retrieved 14 May, 2025, https://www.ghbmc.com/.

[Goldstein-Greenwood, 2022] Goldstein-Greenwood, J. (July 29, 2022). *Detecting Influential Points in Regression with DFBETA(S)*. Retrieved 12 May, 2025, https://library.virginia.edu/data/articles/detecting-influential-points-in-regression-with-dfbetas.

[Goligher et al., 2024] Goligher, E. C., Heath, A., and Harhay, M. O. (2024). Bayesian statistics for clinical research. *The Lancet*, 404(10457):1067–1076. https://doi.org/10.1016/S0140-6736(24)01295-9.

[GraphPad, nd] GraphPad (n.d.). *Ultimate Guide to Survival Analysis*. Retrieved 13 May, 2025, https://www.graphpad.com/guides/survival-analysis.

[International Organization for Standardization [ISO], 2014] International Organization for Standardization [ISO] (2014). *Road Vehicles—Procedure to Construct Injury Risk Curves for the Evaluation of Occupant Protection in Crash Tests.* (ISO/TS 18506:2014). https://www.iso.org/standard/62696.html.

[John Hopkins Medicine, 2025] John Hopkins Medicine (2025). *Head Injury*. Retrieved 21 April, 2025, https://www.hopkinsmedicine.org/health/conditions-and-diseases/head-injury.

[Keyak and Rossi, 2000] Keyak, J. H. and Rossi, S. A. (February, 2000). Prediction of femoral fracture load using finite element models: an examination of stress- and strain-based failure theories. *Journal of Biomechanics*, 33(2):209–214. https://doi.org/10.1016/S0021-9290(99)00152-9.

[Larsson et al., 2021] Larsson, K., Blennow, A., Iraeus, J., Pipkorn, B., and Lubbe, N. (May 24, 2021). Rib cortical bone fracture risk as a function of age and rib strain: Updated injury prediction using finite element human body models. *Front. Bioeng. Biotechnol*, 9. https://doi.org/10.3389/fbioe.2021.677768.

[National Institute on aging, 2022] National Institute on aging (2022). *Falls and Fractures in Older Adults: Causes and Prevention*. Retrieved 10 February, 2025, https://www.nia.nih.gov/health/falls-and-falls-prevention/falls-and-fractures-older-adults-causes-and-prevention.

[Raymond et al., 2009a] Raymond, D., Crawford, G., Van Ee, C., and Bir, C. (2009a). Development of biomechanical response corridors of the head to blunt ballistic temporo-parietal impact. *Journal of Biomechanical Engineering*, 131(9):094506. https://doi.org/10.1115/1.3194751.

[Raymond et al., 2009b] Raymond, D., Van Ee, C., Crawford, G., and Bir, C. (2009b). Tolerance of the skull to blunt ballistic temporo-parietal impact. *Journal of Biomechanics*, 42(15):2479–2485. https://doi.org/10.1016/j.jbiomech.2009.07.018.

[Schachner et al., 2024] Schachner, M., Micorek, J., Luttenberger, P., Greimel, R., Klug, C., and Rajinovic, S. (17 July 2024). *Dynasaur*. (Version 1.4) [Computer Software]. Vehicle Safety Institute TU Graz. https://gitlab.com/VSI-TUGraz/Dynasaur.

[Statistics How To, nd] Statistics How To (n.d.). *Risk Function(Statistics): Definition*. Retrieved 6 May, 2025, https://www.statisticshowto.com/risk-function/.

[Toyota, nd] Toyota (n.d.). *About THUMBS*. Retrieved 14 May, 2025, https://www.toyota.co.jp/thums/about/.

[Viva+, 2025] Viva+ (10 April 2025). *Head Model*. (Version 2.0.1) [Computer Software]. OpenVT. https://openvt.eu/fem/viva/submodels/head.

[Viva+, 2024] Viva+ (25 October 2024). *Validation Catalog*. (Version -) [Computer Software]. OpenVT. https://openvt.eu/fem/viva/vivaplus-validation.

[Viva+, 2022] Viva+ (28 June 2022). *Head*. Retrieved 7 May, 2025, https://vivaplus.readthedocs.io/en/latest/model/body-region/head/.

[Viva+, 2024] Viva+ (9 Setpember 2024). *About VIVA+*. Retrieved 28 April, 2025, https://vivaplus.readthedocs.io/en/latest/about/.

[Wood, 1971] Wood, J. L. (Jan, 1971). Dynamic response of bone human cranial. *Journal of Biomechnics*, 4(1):1–2. https://doi.org/10.1016/0021-9290(71)90010-8.

[World Health Organization, 2024] World Health Organization (1 October 2024). *Ageing and health*. Retrieved 11 March, 2025, https://www.who.int/news-room/fact-sheets/detail/ageing-and-health.

[World Health Organization, 2021] World Health Organization (26 April 2021). *Falls*. Retrieved 21 April, 2025, https://www.who.int/news-room/fact-sheets/detail/falls.

[Zienkiewicz et al., 2013] Zienkiewicz, O., Taylor, R., and Zhu, J. (2013). *The Finite Element Method: Its Basis and Fundamentals*. Butterworth-Heinemann. https://doi.org/10.1016/C2009-0-24909-9.

Appendix

A Scatter Plots of the Wood Data

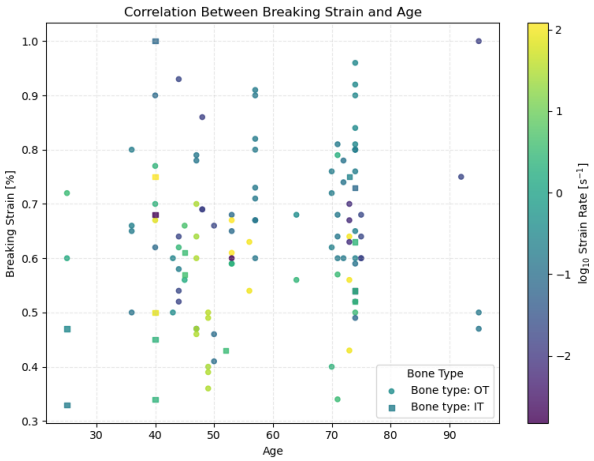

Figure A.1: Breaking strain plotted against age for the [Wood, 1971] data. The gradient shows log_{10} strain rate.

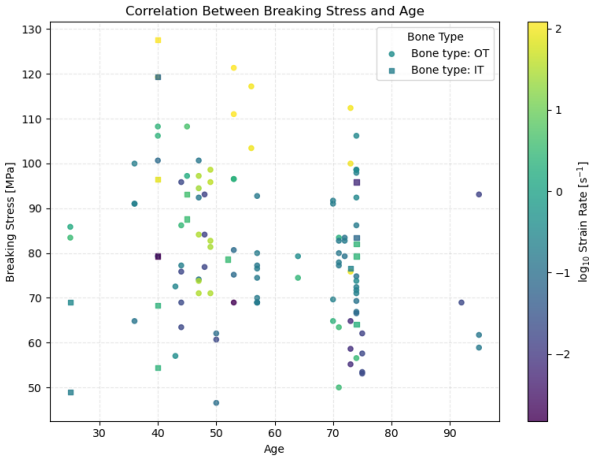

Figure A.2: Breaking stress plotted against age for the [Wood, 1971] data. The gradient shows log_{10} strain rate.

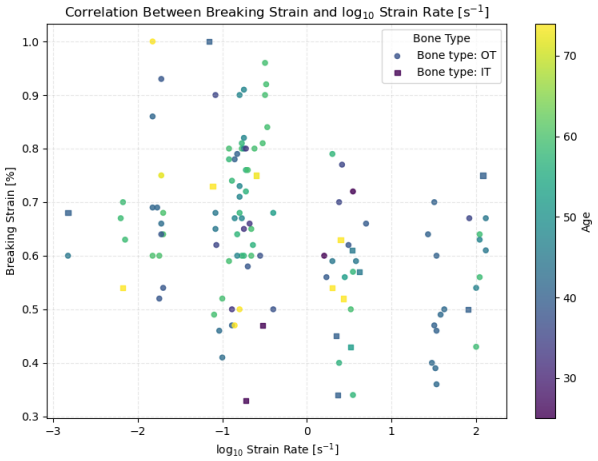

Figure A.3: Breaking strain plotted against log_{10} strain rate for the [Wood, 1971] data. The gradient shows age.

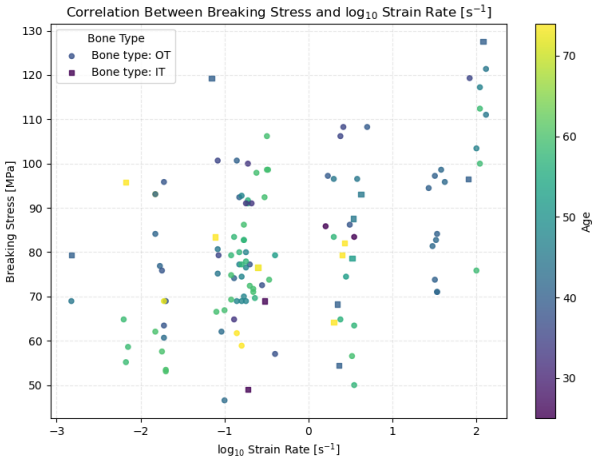

Figure A.4: Breaking stress plotted against log_{10} strain rate for the [Wood, 1971] data. The gradient shows age.

B Posteriors For Levels In Bayesian Models

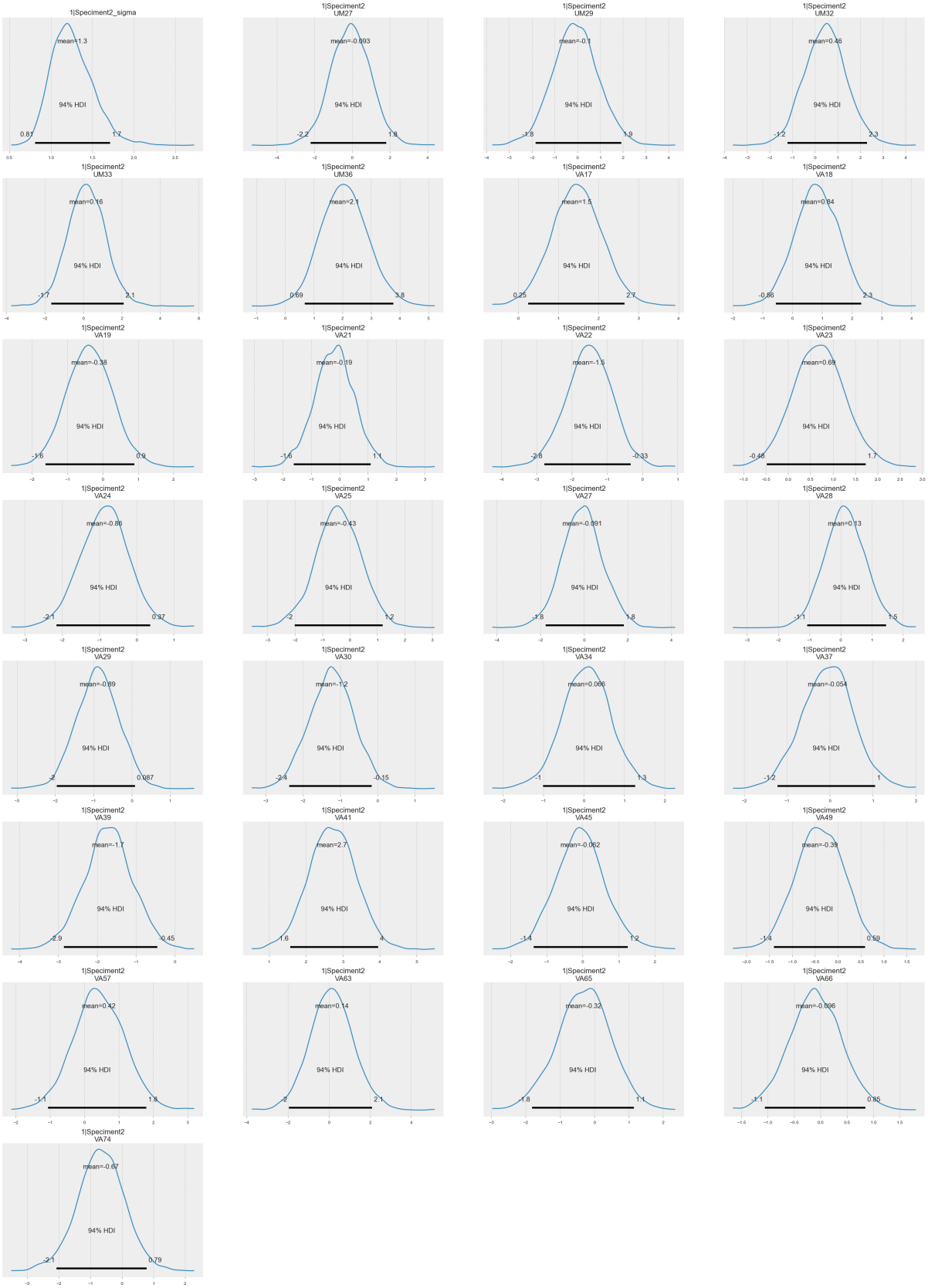

Figure B.1: Posterior for the levels within the Bayesian model predicting modulus of elasticity.

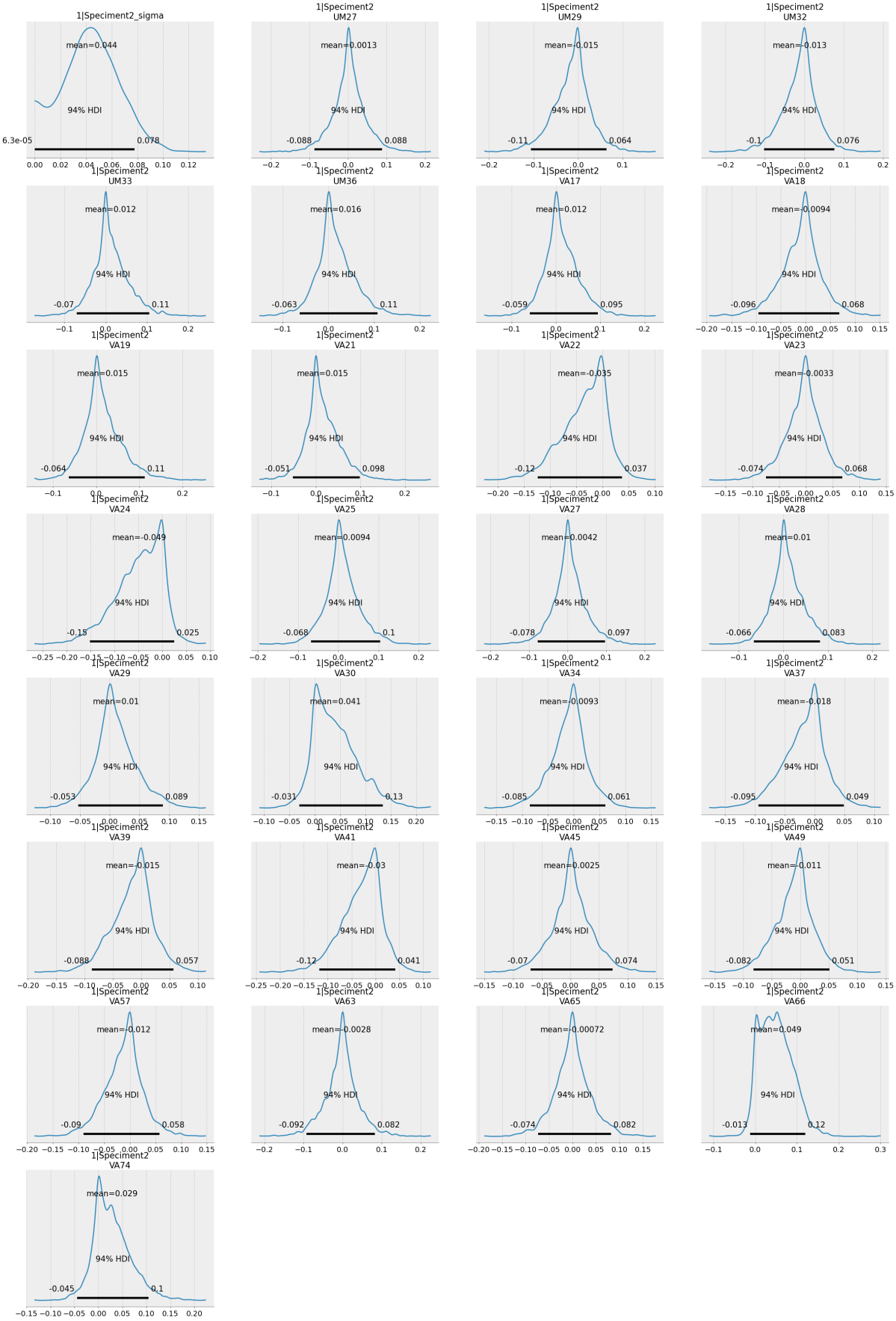

Figure B.2: Posterior for the levels within the Bayesian model predicting braking strain.

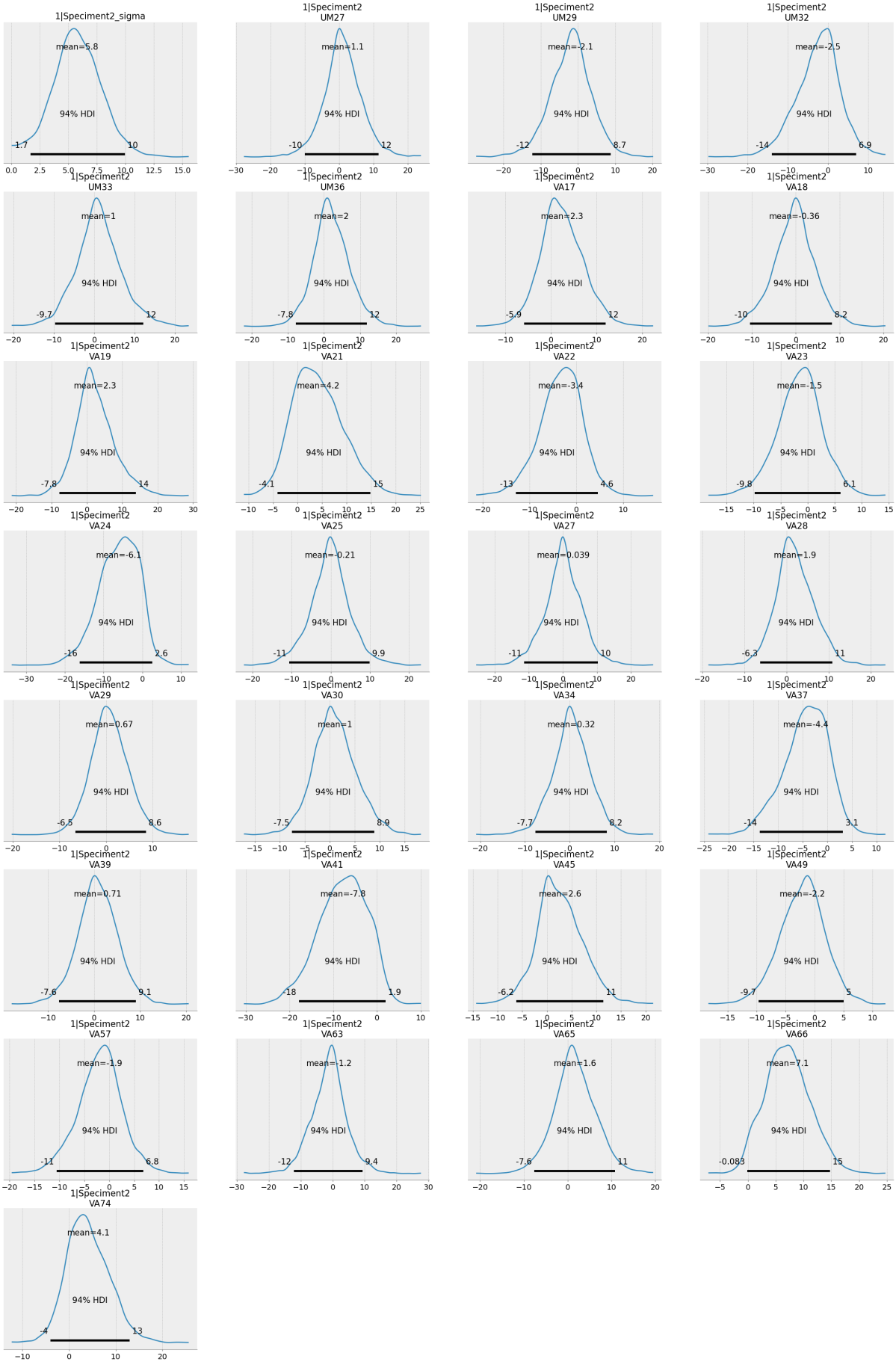

Figure B.3: Posterior for the levels within the Bayesian model predicting braking stress.

C DFBETAS for age and sex

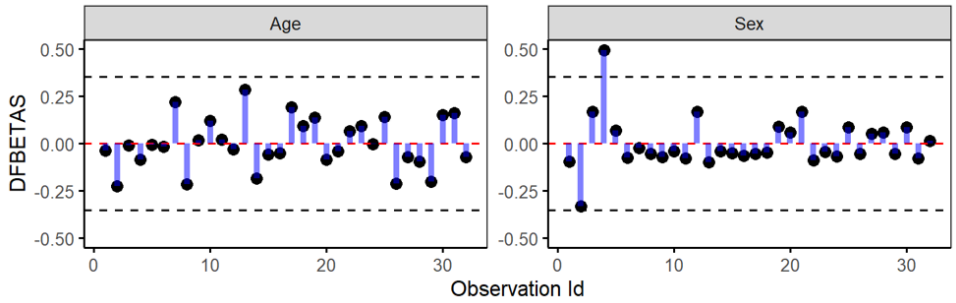

Figure C.1: The DFBETAS for age and sex calculated with true total braking strain.

D COX regression results

Table D.1: The complete value from the true total breaking strain calculated with COX regression.

Parameters	**coef**	**exp(coef)**	**se(cef)**	**z**	**Pr($>|z|$)**
Age	-0.01677	0.98337	0.0121	-1.385	0.166
Bone	1.1955	3.3052	0.69901	1.71	0.0872
as.factor(Part)1	0.72845	2.07186	0.81762	0.891	0.373
as.factor(Part)2	0.6885	1.99074	0.88535	0.778	0.4368
Sex	-1.88072	0.15248	0.82713	-2.274	0.023*

E Quality check of the risk function

Table E.1: The range for quality for risk curves.

Quality index	**Relative size of the 95% confidence interval**
Good	from 0 to 0.5
Fair	from 0.5 to 1
Marginal	from 1 to 1.5
Unacceptable	over 1.5

Table E.2: Quality check- 50-year-old.

Injury Criteria	**Risk (%)**	**Estimate**	**Lower CI**	**Upper CI**	**Relative CI size**	**Quality Index**
True breaking strain (age as covariate)	5	0.004503	0.003943	0.005065	0.249	Good
	25	0.006404	0.006053	0.006768	0.112	Good
	50	0.006289	0.005929	0.006663	0.116	Good

Table E.3: Quality check for Male.

Injury Criteria	**Risk (%)**	**Estimate**	**Lower CI**	**Upper CI**	**Relative CI size**	**Quality Index**
True breaking strain (sex as covariate)	5	0.0039	0.0032	0.0046	0.363	Good
	25	0.0055	0.0048	0.0063	0.289	Good
	50	0.0054	0.0047	0.0062	0.290	Good

F Strain Rate Curves

Figure F.1: Stress-strain curve for a dogbone specimen modeled using the Male 50 material card.

Figure F.2: Stress-strain curve for a dogbone specimen modeled using the Female 80 material card.

Figure F.3: Stress-strain curve for a dogbone specimen modeled using the Female 50 material card.

G 99 Percentile Strain

Table G.1: 99 Percentile Strains at assumed fracture.

PMHS ID	Velocity [m/s]	Fracture (yes/no)	Strain [%] pre-project	Strain [%] base	Strain [%] scaled	Strain [%] aged
2426 (HS/LS)	32.1/22.2	y/n	0.31/0.19	0.33/0.19	0.41/0.29	0.42/0.30
2904 (HS/LS)	31.9/17.3	n/n	0.32/0.06	0.32/0.06	0.40/0.09	0.42/0.10
2908 (HS/LS)	35.1/19.6	y/n	0.29/0.14	0.90/0.16	0.66/0.26	0.69/0.26
2939 (HS/LS)	34.4/16.3	n/n	0.86/0.16	0.89/0.18	0.53/0.03	0.54/0.03
2965 (HS/LS)	35.2/18.0	y/n	0.36/0.13	0.39/0.15	0.22/0.20	0.22/0.20
2978 (HS/LS)	32.4/19.5	y/y	0.18/0.12	0.19/0.13	0.07/0.00	0.07/0.00

Table G.2: Risk of Fracture for 99th percentile, calculated with variables depending on age (50 or 80 years).

PMHS ID	Velocity [m/s]	Fracture in experiment (yes/no)	Risk of Fracture scaled [%]	Risk of Fracture aged [%]
2426 (L/R)	32.1/22.2	y/n	47.03/26.58	53.28/31.53
2904 (L/R)	31.9/17.3	n/n	45.94/3.04	54.00/3.70
2908 (L/R)	35.1/19.6	y/n	81.44/21.36	88.55/25.67
2939 (L/R)	34.4/18.0	n/n	0.36/65.69	0.43/72.25
2965 (L/R)	35.2/18.0	n/y	13.72/15.86	16.34/18.80
2978 (L/R)	32.4/19.5	y/y	1.82/0.00	2.19/0.00

The risk of fracture was calculated for the 99th percentile strain, the result was lower values for risk of fracture compared to the max strain, but otherwise the relation to the real experiment was about the same.

H Speciemen 2427

Table H.1: Scaling factor 2427.

PMHS ID	Scaling Factor
2427	0.87686

Table H.2: Maximum strains at predicted fracture time for 2427.

PMHS ID	Velocity [m/s]	Fracture (yes/no)	Strain [%] pre-project	Strain [%] base	Strain [%] scaled	Strain [%] aged
2427 (L/R)	34.2/23.4	y/y	0.14/0.02	0.14/0.02	0.00/0.01	0.00/0.01

Table H.3: Risk of Fracture for 2427, calculated with variables depending on age (50 or 80 years).

PMHS ID	Percentile	Fracture in experiment (yes/no)	Risk of Fracture scaled [%]	Risk of Fracture aged [%]
2427 (L/R)	100	y/y	0.00/0.01	0.01/0.01
2427 (L/R)	99	y/y	0.00/0.00	0.00/0.00

I Simulation compared to experiment

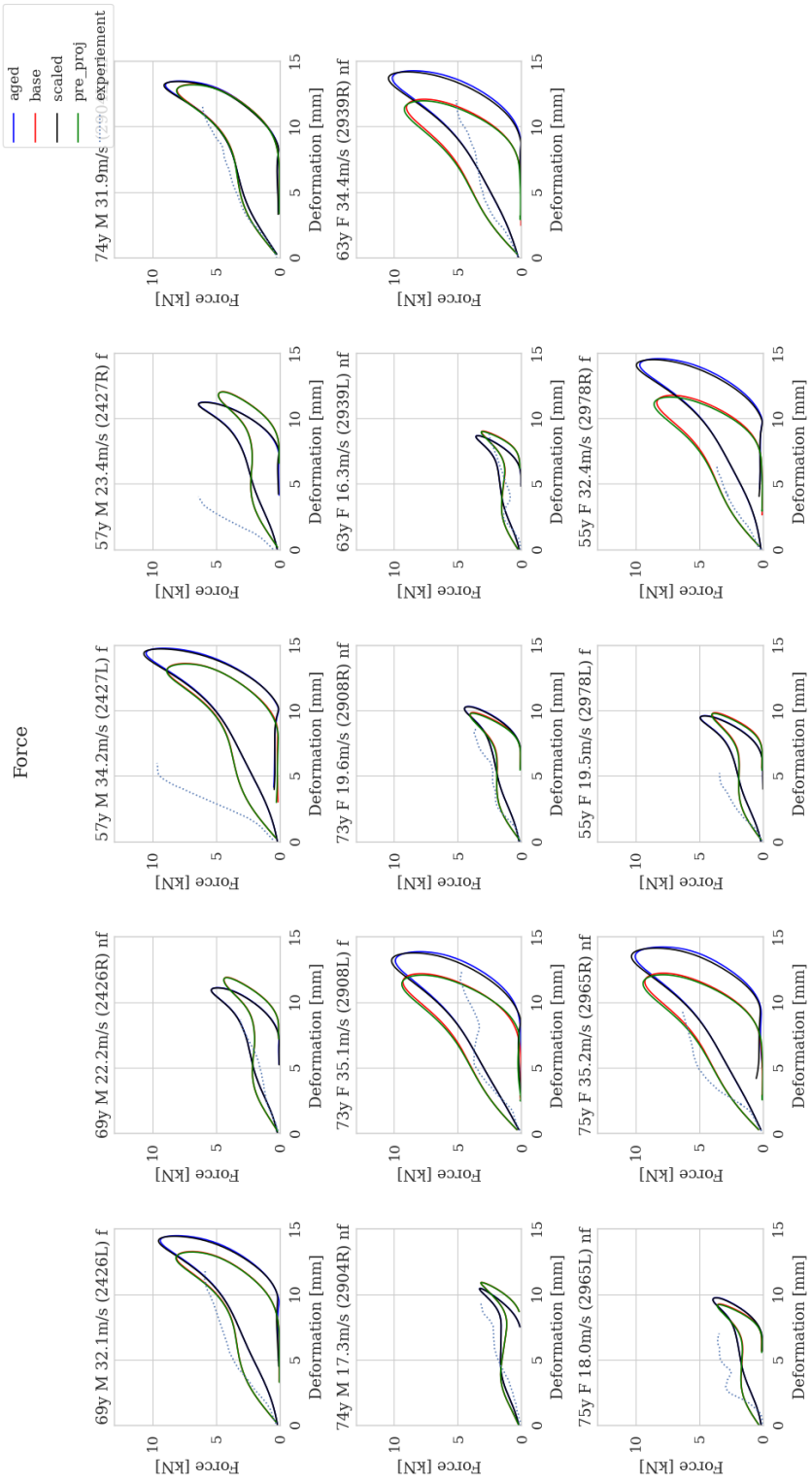

Figure I.1: The simulations compared to the experiment.